Chemical Geology 294-295 (2012) 51–62

Contents lists available at SciVerse ScienceDirect

Chemical Geology

journal homepage: www.elsevier.com/locate/chemgeo

Research paper

The origin of NO_3^- and N_2 in deep subsurface fracture water of South Africa

Bianca J. Silver [a,b,h], R. Raymond [a,h], Daniel M. Sigman [a], Masha Prokopeko [c], Barbara Sherwood Lollar [d,h], Georges Lacrampe-Couloume [d,h], Marilyn L. Fogel [e,h], Lisa M. Pratt [f,h], Liliana Lefticariu [f,g,h], T.C. Onstott [a,h,*]

[a] Princeton University, Dept. of Geosciences, Guyot Hall, Princeton, NJ 08544, USA
[b] ARCADISU.S., Inc. 8 South River Road, Cranbury, NJ 08512, USA
[c] University of Southern California. Dept. of Earth Sciences, Zumberge Hall of Science (ZHS) 3651 Trousdale Pkwy, Los Angeles, CA 90089-0740, USA
[d] University of Toronto, Dept. of Geology, 22 Russell St., Toronto, ON, Canada M5S 3B1
[e] Carnegie Institution of Washington, Geophysical Laboratory, Washington, DC 20005-1933, USA
[f] Department of Geological Sciences, Indiana University, Bloomington, IN 47405, USA
[g] Department of Geology, Southern Illinois University, Carbondale, IL 62901-6899, USA
[h] Indiana Princeton Tennessee Astrobiology Initiative (IPTAI), NASA Astrobiology Institute, Indiana University, Bloomington, IN, USA

A R T I C L E I N F O

Article history:
Received 28 June 2011
Received in revised form 11 November 2011
Accepted 16 November 2011
Available online 25 November 2011

Editor: J.D. Blum

Keywords:
N isotopes
Deep
Subsurface microbial ecosystems
Radiolysis
N cycle

A B S T R A C T

Deep (>0.8 km depth) fracture water with residence time estimates on the order of several Ma from the Witwatersrand Basin, South Africa contains up to 40 μM of NO_3^-, up to 50 mM N_2 (90 times air saturation at surface) and 1 to ~400 μM NH_3/NH_4^+. To determine whether the oxidized N species were introduced by mining activity, by recharge of paleometeoric water, or by subsurface geochemical processes, we undertook N and O isotopic analyses of N species from fracture water, mining water, pore water, fluid inclusion leachate and whole rock cores.

The NO_2^-, NO_3^- and NH_3/NH_4^+ concentrations of the pore water and fluid inclusion leachate recovered from the low porosity quartzite, shale and metavolcanic units were ~10^4 times that of the fracture water. The $\delta^{15}N$–NO_3^- and $\delta^{18}O$–NO_3^- of the pore water and fluid inclusion leachate, however, overlapped that of the fracture water with the $\delta^{15}N$–NO_3^- ranging from 2 to 7‰ and the $\delta^{18}O$–NO_3^- ranging from 20 to 50‰. The $\delta^{15}N$–NO_3^- of the mining water ranged from 0 to 16‰ and its $\delta^{18}O$–NO_3^- from 0 to 14‰ making the mining water NO_3^- isotopically distinct from that of the fracture, pore and fluid inclusion water. The $\delta^{15}N$–N_2 of the fracture water and the $\delta^{15}N$–N from the cores ranged from −5 to 10‰ and overlapped the $\delta^{15}N$–NO_3^-. The $\delta^{15}N$–NH_4^+ of the fracture water and pore water NH_3/NH_4^+ ranged from −15 to 4‰. Although the NO_3^- concentrations in the pore water and fluid inclusions were high, mass balance calculations indicate that NO_3^- accounts for ≤10% of the total rock N, whereas NH_3/NH_4^+ trapped in fluid inclusions or NH_4^+ present in phyllosilicates account for ≥90% of the total N.

Based on these findings, the fluid inclusion NO_3^- appears to be the source of the pore water and fracture water NO_3^- rather than paleometeoric recharge or mining contamination. Irradiation experiments indicate that radiolytic oxidation of NH_3 to NO_3^- can explain the fluid inclusion NO_3^- concentrations and, perhaps, its isotopic composition, but only if the NO_3^- did not attain isotopic equilibrium with the hydrothermal fluid 2 billion years ago. The $\delta^{15}N$–N, $\delta^{15}N$–N_2 and $\delta^{15}N$–NH_4^+ suggest that the reduction of N_2 to NH_4^+ also must have occurred in the Witwatersrand Basin in order to explain the abundance of NH_4^+ throughout the strata. Although the depleted NO_3^- concentrations in the fracture water relative to the pore water are consistent with microbial NO_3^- reduction, further analyses will be required to determine the relative importance of biological processes in the subsurface N cycle and whether a complete subsurface N cycle exists.

1. Introduction

With the discovery of widespread microbial life in the deep subsurface, the question of nutrient availability becomes critical to understanding the limits of this ecosystem. In the case of marine sediments, Lipp et al. (2008) reported that the total lipid concentration, a proxy for living biomass, was correlated with the total organic matter concentration (TOC), such that cellular densities diminished to ~10^6 cells g^{-1} for sediment with TOC of ~0.2%. A number of recent studies have shown, however, that H_2-producing water–rock interactions provide the energy for subsurface autotrophic microbial metabolism deep in the earth's crust (Stevens and McKinley, 1995; Kelley et al., 2001; Lin et al., 2005b, 2006) and that acetogens could provide the organic carbon substrate necessary to support aceticlastic

* Corresponding author at: Dept. of Geosciences, Princeton University, Princeton, NJ 08544, USA. Tel.: +1 609 258 7678; fax: +1 609 258 1274.
E-mail addresses: Bianca.silver@arcadis-us.com (B.J. Silver), prokopen@usc.edu (M. Prokopeko), bslollar@chem.utoronto.ca (B. Sherwood Lollar), m.fogel@gl.ciw.edu (M.L. Fogel), prattl@indiana.edu (L.M. Pratt), tullis@princeton.edu (T.C. Onstott).

0009-2541/$ – see front matter © 2011 Elsevier B.V. All rights reserved.
doi:10.1016/j.chemgeo.2011.11.017

heterotrophs (Stevens and McKinley, 1995; Stevens, 1997). The principal N substrate for subsurface ecosystems could be NH_3/NH_4^+ originating from deamination of organic photosynthate or from deep-seated N-containing fluids from silicates (Mysen and Fogel, 2010). Determining the origin and form of N available to the deep biosphere community is critical for understanding how it may influence and limit autotrophic microbial abundance in the deep terrestrial subsurface. Significant N_2 concentrations have been discovered in gas reservoirs <1 km depth that are typically associated with high ^4He, indicating a crustal origin and long subsurface residence time for N_2 (Ballentine and Sherwood Lollar, 2002). In deeper crustal environments (T = 400–700 °C) N_2 is the dominant N fluid species unless low fO_2 conditions stabilize NH_3 (Haendel et al., 1986; Bebout and Fogel, 1992). The migration of N_2 from deeper to shallower crustal levels could provide an alternative N source for deep subsurface N_2-fixing microbial communities in the absence of NH_3. Autotrophs that are capable of N_2 fixation, such as *Candidatus Desulforudis audaxviator* (Chivian et al., 2008), have also been reported from deep subsurface samples despite the fact that N_2 fixation is energetically costly.

NO_3^- is generally accepted to be an important source of energy and nutrients for microorganisms in shallow aquifers and marine sediments, but not for deeper settings. D'Hondt et al. (2004), however, identified NO_3^- (≤30 μM) in the pore water of seafloor sediments near their contact with the underlying basaltic crust and conjectured that "the transport of O_2 and NO_3 through the underlying basaltic aquifer sustains aerobic and nitrate-reducing prokaryotic communities in the deepest (11 to 35 Ma) sediments of these sites, although anaerobic communities are active in the overlying sediment". Much higher NO_3^- concentrations have been reported in the pore water of ultra-high-pressure metamorphic rocks in China (~20 mM) (Zhang et al., 2005) and in the fluid inclusions in ~2.0 Ga hydrothermal veins of the Omai Au deposit in South America (≤15 mM) (Voicu and Hallbauer, 2005) and the Witwatersrand Basin of South Africa (≤70 mM) (Frimmel et al., 1999). Lower NO_3^- concentrations, ≤40 μM, have also been reported for the fracture water emanating from mine boreholes at 0.8 to 3.5 km depth in the Witwatersrand Basin, which is believed to be a mixture of paleometeoric water and ~2.0 Ga hydrothermal fluid (Onstott et al., 2006). Caution must be exercised, however, when examining NO_3^- in a mining environment as Onstott et al. (2003), Stroes-Gascoyne and Gascoyne (1998), Gascoyne and Thomas (1997) and Stotler et al. (2009) have all stressed that the NO_3^- may originate from the explosives used in mining.

A possible origin for these reported deep NO_3^- occurrences is suggested by irradiation studies of NH_3-bearing water solutions that have measured the production of NH_2O_2 (Pagsberg, 2001), N_2H_4 (Rigg et al., 1952), NO_2^- (Dwibedy et al., 1996) and NO_3^- (Shin et al., 2001). If NO_3^- and NO_2^- are produced within the subsurface from irradiation of NH_3, then they could provide an alternative source of N, an energy-rich electron acceptor and could, in principal, sustain a complete subsurface N cycle.

This study, therefore, sought to determine to what extent the three principal N species, NO_3^-, NH_3 and N_2, observed in the Witwatersrand Basin fracture water were derived from mining contamination, from the surface biosphere by recent meteoric recharge, from Archean organic-rich shale, or from a ~2.0 Ga hydrothermal fluid. This was done by performing N and O isotopic analyses on cores collected from the lithological units in contact with these fractures, the organic-rich Kimberly Shale, the Ventersdorp Supergroup metavolcanics and the Witwatersrand Supergroup quartzite. In addition NH_3 irradiation experiments on anaerobic water were performed to test the possibility of radiolytically produced NO_3^-.

2. Geologic setting

The Witwatersrand Basin, located in the center of the Kaapvaal Craton, is 300 km long along a NE–SW axis and 100 km wide, and formed 3.1 to 2.7 byr ago. The core samples for this study were collected during exploration coring from the Evander and Kloof Au mines. Evander Au Mine is located on the easternmost edge of the Witwatersrand Basin where the 2.9 Ga Witwatersrand Supergroup is overlain by the 2.7 Ga old Ventersdorp Supergroup. At this location the Upper Witwatersrand Group stratigraphic column includes the 60 m thick Booysens/Kimberley Shale Formation underlain by the 30 m thick Krugersdorp Quartzite Formation and overlain the 6 m thick Kimberley reef of the 14 m thick Kimberley–Elsburg Quartzite Formation (Tweedie, 1986). Kloof Au Mine (S 26°26′; E 27°34′) is located southwest of Johannesburg where the contact between the Ventersdorp Supergroup and the Upper Witwatersrand Group is mined. Metamorphic mineral assemblages are consistent with lower greenschist facies with maximum temperatures of 300 ± 50 °C and pressures of 2.5–3 kbar (Phillips, 1988; Wallmach and Meyer, 1990). Fluid inclusion studies indicate a maximum temperature of 250 °C (Hallbauer and Kable, 1979; Hallbauer and Von Gehlen, 1983; Hallbauer, 1986).

3. Materials and methods

3.1. Core collection

On August 13, 2002 at the 24th level, 1.83 km bls., of #2 shaft of Evander Au mine (S 26°30′36″; E 29°08′40″) a very short exploratory borehole was drilled downwards for 20 m through the Kimberley reef and the resulting quartzite and conglomerate rock core, labeled EV224, was collected. No fracture water was associated with the EV224 borehole; only mining water was obtained. On October 25, 2002 during an exploratory coring operation on the 18th level of the #8 shaft of Evander Au mine (S 26°27′13″; E 29°03′56″), 1.83 km bls., a 2 m core of the Kimberley–Elsburg Quartzite Formation, labeled as EV818, was collected from a vertical borehole at a depth of 60 m below the tunnel floor. This sampling was followed by collection of numerous fracture water samples. Samples were collected of the calcareous siltstone and the upper laminated sections of the Kimberley Shale, as well as from the quartzite and conglomerate overlying and underlying it. These samples were taken from an exploration core through the Upper Witwatersrand Group drilled from #3 shaft of Evander Au mine (S 26°31′5″; E 29°07′40″) at a depth comparable to that of the other cores, and, hence, referred to as core EV3.

On July 31, 2003, several core samples along with fracture water and mine water samples were collected from a horizontal borehole drilled into a water bearing fracture at the 39th level, 3.1 km bls., of the #7 shaft of Kloof Au mine (S 26°26′42″; E 27°33′59″). Rock cores, labeled KL739, were collected from the lower greenschist facies, tholeiitic, Ca-rich, porphyritic flood basalt of the Klipriviersberg Group of the Ventersdorp Supergroup (van der Westhuizen et al., 1991).

All freshly drilled rock cores were immediately stored in sterile Whirlpak bags and frozen on dry ice. The rock cores were subsequently shipped frozen to Princeton University where they were stored in a −80 °C freezer. EV3 was collected from the Evander Au mine core library after storage for several weeks and, thus, was not suitable for pore water analyses, but as it is the only organic carbon bearing shale unit in the Witwatersrand strata, it was collected to measure the isotopic composition of any organic N.

3.2. Fracture water sample collection

Mining water was collected from the EV224, and mining water and fracture water were collected from the EV818 and KL739 coring operations on August 13, 2002, October 25, 2002 and July 31, 2003, respectively. An autoclaved Margot-type expansion plug connected to a sampling manifold constructed of Delran plastic and equipped with quick-connect release valves and sterile tubing with a syringe tip was used to collect water and gas samples without exposing them to the mine air, following the procedures described in Onstott et al. (2006).

3.3. Pore water, fluid inclusion, exchangeable NH_4^+ extractions

Rock cores were 45 to 50 mm in diameter and were split into 20 g nugget (internal) and 20 g paring (outer rim) portions using a custom-made rock splitter. Within an anaerobic glove bag, the nuggets and parings were aseptically broken into smaller pieces and placed into 50 mL centrifuge tubes with 40 mL of deionized, degassed, sterile water. The samples were placed on a rotisserie shaker in the anaerobic glove bag for 5 days. This pore water leachate was frozen and saved for concentration (NH_4^+ and NO_3^-) and isotopic analysis ($\delta^{15}N$–NO_3^-, $\delta^{18}O$–NO_3^- and $\delta^{15}N$–NH_4^+). The rock fragments were subsequently pulverized, sieved at mesh number 200 (pore size of 75 μm) and placed in 40 mL of deionized, degassed water and set on the shaker for 5 days with all steps taking place in the anaerobic glove bag. This fluid inclusion leachate was frozen and set aside for concentration (NH_4^+ and NO_3^-) and isotopic ($\delta^{15}N$–NO_3^-, $\delta^{18}O$–NO_3^- and $\delta^{15}N$–NH_4^+) measurements. These same steps were first performed without rock to determine the trace amounts of NO_3^- present in the procedure. Multiple tests revealed that certain 50 mL centrifuge tube caps contained significant NO_3^- contamination, and the caps that yielded no detectable NO_3^- contamination were then selected for the extraction process.

To determine the exchangeable NH_4^+ in the residual powder, 20 mL of degassed, pH 7, 2 M KCl was added. The solution was shaken for 1 h in the anaerobic glove bag, centrifuged for 5 min at 3400 rpm, the leachate removed, the powder rinsed with 10 mL of deionized, degassed H_2O and centrifuged for 15 min. The deionized, degassed H_2O step was repeated. The DI H_2O rinses were added to the 20 mL KCl solution for a total volume of 40 mL.

3.4. Dissolved N species analyses

All NO_3^-, NO_2^- and NH_4^+ concentrations for mining water, fracture water, pore water and fluid inclusion extract samples were analyzed at Princeton University (Tables 1–3). NO_3^- and NO_2^- were measured by ion chromatography (DX-320, Dionex, Sunnyvale, CA) using EG40 and LC25 columns and an AS40 autosampler with detection limits of 0.2 and 0.1 μM, respectively. Pore water and fluid inclusion extract NO_3^- concentrations were also measured in duplicate by reduction to nitric oxide (NO) in a heated solution of acidic V^{3+} followed by chemiluminescent detection of the NO (Braman and Hendrix, 1989) with a detection limit of 0.01 μM for 2–3 mL injections. NH_4^+ concentrations were determined using the Nesslerization method (Eaton et al., 1995) with detection limits of 1 μM and a relative standard deviation of 10% based on a four point calibration curve.

NO_3^-, NO_2^- and NH_4^+ measurements for the extracts were converted into pore water and fluid inclusion concentrations using the following relationship,

$$[N_x]_{PW,FI} = (W_l/W_r)\cdot([N_x]_{meas}/MW_x)\cdot(r_{rock}/\theta_{rock}) \quad (1)$$

where $[N_x]_{PW,FI}$ is the concentration of NO_3^-, NO_2^- or NH_4^+ in the pore water or fluid inclusion (in mM) (Table 3), W_l is the volume of the D.I. water extract (40 mL), W_r is the mass of the rock being extracted (2 to 6 g), $[N_x]_{meas}$ is the NO_3^-, NO_2^- or NH_4^+ concentration in the extract (in mg L^{-1}), ρ_{rock} is the density of the rock (in grams cm^{-3}), θ_{rock} is the

Table 2
Mining water geochemistry and nitrogen and oxygen isotopic composition for dissolved NO_3^-.

Sample	NO_3 (μM)	$\delta^{15}N$ NO_3 (‰)	$\delta^{18}O$ NO_3 (‰)	NH_3/NH_4^+ (μM)	Na (mM)
KL 739 SW A	1354 ± 80	6.8	14.2	14.3	15
KL 739 SW B	1701 ± 75	5.1	14.0	37.8	15
KL739 DW2073103	0.82 ± 0.20	8.2	3.7	11.8	15
DR938CH091202	52.7 ± 0.1	16.5	0.4	90.5	3
DR938 TW	5.34 ± 0.08	0.6	5.0	0.7	5
DR 938 TW	5.20 ± 0.07	0.7	5.1	n.a.	5

Table 1
Fracture water analyses.

Sample[a]	$\delta^{15}N$ N_2 (‰)[b]	% atm.	N_2[c] (μM)	$\delta^{15}N$ N_2[c] (‰)	NO_3^- (μM)	$\delta^{15}N$ NO_3^- (‰)[b]	$\delta^{18}O$ NO_3^- (‰)[b]	NH_3/NH_4^+ (μM)	$\delta^{15}N$ NH_3 (‰)[b]	Na (mM)[d]	$\delta^{18}O$ H_2O[d]	Age (Ma)
BE116 031401 IDW	−0.9 ± 0.1	69.0	1102	−1.3 ± 0.1	1.04 ± 0.01	5.9	30.7	0.71	n.a.	34	−6.00	2.0[f]
BE116 H1 031601	0.8 ± 0.1	67.0	636	4.1 ± 0.1	1.04 ± 0.01	n.a.	n.a.	27.5	−6.0	32	−5.85	2.0[f]
BE325 FW 032701	−0.8 ± 0.1	18.9	94	−0.9 ± 0.1	2.80 ± 0.03	5.2	30.8	2.14	n.a.	35	−6.71	5.0[f]
BE327 H3 032701	−0.8 ± 0.1	18.4	214	−0.9 ± 0.2	1.50 ± 0.01	5.5	30.9	213	n.a.	32	−6.66	3.5[f]
MS151 FW 022202	0.3 ± 0.1	47.8	592	2.4 ± 0.1	37.5 ± 2.33	9.9	24.9	120	n.a.	56	−7.19	1.3
MM51870 030402	0.5 ± 0.1	50.3	860	2.9 ± 0.1	4.08 ± 0.01	2.3	20.4	28.6	3.3	44	−6.52	1.6
EV818 FW 030601	2.9 ± 0.1	27.3	473	5.8 ± 0.1	0.20 ± 0.01	n.a.	n.a.	31.6	n.a.	89	−10.2	9.5[f]
EV818 FW 051001	n.a.	n.a.	n.a.	n.a.	4.90 ± 0.01	18.7	25.9	71.4	n.a.	83	−10.5	7.3
EV818 FW 062101	n.a.	n.a.	n.a.	n.a.	5.40 ± 0.01	5.1	26.9	40.2	n.a.	78	−10.9	6.0
EV522 FW 030801	1.6 ± 0.1	47.3	627	1.9 ± 0.1	0.35 ± 0.04	n.a.	n.a.	8.05	n.a.	24	−5.63	0.7
EV522 H1 041801	1.8 ± 0.1	19.9	1450	4.1 ± 0.1	0.51 ± 0.04	n.a.	n.a.	28.6	n.a.	33	−6.48	1.2[f]
EV219 H1 030901	1.6 ± 0.2	34.3	14,118	1.7 ± 0.2	0.18 ± 0.01	n.a.	n.a.	4.28	n.a.	17	−4.98	7.7
EV219 H5 030901	n.a.	n.a.	52,800	n.a.	1.22 ± 0.04	6.8	34.0	n.a.	n.a.	15	−4.92	0.8
DR983 H3 110701	−0.1 ± 0.1	13.1	2674	−0.1 ± 0.1	0.80 ± 0.04	0.9	24.1	2.86	n.a.	14	−5.01	3.5
DR938 H1 082001	0.8 ± 0.1	72.3	1430	4.2 ± 0.1	0.16 ± 0.01	n.a.	n.a.	27.8	n.a.	1.7	−4.31	n.a.
DR938 CH 110701	0.8 ± 0.1	77.8	806	5.1 ± 0.1	2.23 ± 0.04	n.a.	n.a.	7.14	n.a.	3.8	−4.68	0.001[e]
KL441 H3 111401	0.8 ± 0.1	44.1	381	0.8 ± 0.1	0.13 ± 0.04	n.a.	n.a.	24.3	n.a.	22	−5.03	3.9[f]
KL739 FW 062901	0.9 ± 0.2	8.5	473	1.0 ± 0.2	0.97 ± 0.01	n.a.	n.a.	14.3	n.a.	95	−7.24	20[f]
MP104 E65XC H1	0.3 ± 0.2	24.2	251	1.3 ± 0.2	0.54 ± 0.03	n.a.	n.a.	406	−14.9	52	−6.82	20[f]
DR548 FW 090901	n.a.	n.a.	1170	n.a.	0.16 ± 0.01	n.a.	n.a.	25.7	n.a.	723	−12.3	15

[a] Boreholes MS151, MM5, BE116, BE325, BE327, EV818, and EV522 are situated in Witwatersrand Supergroup quartzite. Borehole EV219 is situated in Ventersdorp Supergroup metadiabase. Boreholes KL441, KL739, DR938 H1, DR938 CH and MP104 are situated in Ventersdorp Supergroup metavolcanic. DR938 H3 intersects both the Ventersdorp Supergroup and the Witwatersrand Supergroup.

[b] $\delta^{15}N$ values for N_2, NO_3^- and NH_3 are expressed in ‰ with respect to atmospheric N_2 and $\delta^{18}O$ for NO_3^- is expressed in ‰ with respect to V-SMOW.

[c] N_2 concentrations and $\delta^{15}N$ N_2 were corrected for air contamination based on Eqs. (3) and (4) (see text).

[d] Na^+ concentrations and $\delta^{18}O$ for water are summarized in Onstott et al. (2006), Ward et al. (2004) and Lippmann et al. (2003).

[e] This sample's age was determined by AMS analyses of the DIC. $\Delta^{14}C = -420$‰ and $\delta^{13}C = -10.1$‰, DIC = 0.63 mM. Assuming the $\delta^{13}C$ of recharge = −17‰ and the $\delta^{13}C$ of the Transvaal Group dolomite = −0.55‰ (Bau et al., 1999), the ^{14}C age corrected for dead carbon addition is 1022 years.

[f] These water ages were reported by Lippmann et al. (2003) and Lin et al. (2006). The remaining water ages are based upon the He concentrations, uncorrected for diffusive loss, but calculated according to the same Lippmann et al. (2003) model used for the other water ages (Supplemental Dataset).

Table 3
Pore water, fluid inclusion and exchangeable NH_4^+ ($NH_4{}^+{}_{ex}$) analyses.

Sample[a]	NO_3^- (μM)[b]	NO_3^- (mM)[c]	$\delta^{15}N$ NO_3^- (‰)	$\delta^{18}O$ NO_3^- (‰)	NO_2^- (μM)[b]	NO_2^- (mM)[c]	NH_3/NH_4^+ (μM)[b]	NH_3/NH_4^+ (mM)[c]	$\delta^{15}N$ NH_3 (‰)	Na (mM)	$NH_4{}^+{}_{ex}$ (10^{-3} mol kg^{-1})
KL739 A3N PW	1.33 ± 0.06	4.32	−0.1	23.7	0.43	1.40	22 ± 5	59	n.a.	964	N/A
KL739 A3P PW	0.87 ± 0.01	1.93	0.1	28.3	0.48	1.06	1.6 ± 1.6	4.7	n.a.	1131	N/A
KL739 B3N PW	0.71 ± 0.09	1.19	5.7	23.9	<dl	<dl	17 ± 1	28	n.a.	937	N/A
KL739 B3P PW	0.54 ± 0.04	0.96	n.a.	n.a.	<dl	<dl	18 ± 3	32	n.a.	836	N/A
KL739 B6P PW	0.65 ± 0.05	4.04	n.a.	n.a.	<dl	<dl	13 ± 2	39	n.a.	581	N/A
KL739 B6N PW	0.56 ± 0.02	3.83	n.a.	n.a.	0.28	1.88	19.07 ± 0.01	79	n.a.	589	N/A
KL739 B10N PW	1.18 ± 0.01	3.52	2.0	28.4	0.45	1.35	10 ± 1	17	n.a.	1041	N/A
KL739 B10P PW	1.06 ± 0.01	2.23	2.9	27.9	0.42	0.89	27 ± 2	57	n.a.	951	N/A
EV818 P PW	12.5 ± 0.11	17.0	−0.3	31.1	<dl	<dl	31 ± 35	26	n.a.	358	N/A
EV818 N PW	4.52 ± 0.01	7.95	2.4	26.8	<dl	<dl	30 ± 9	59	n.a.	338	N/A
EV818 BN2 PW	1.90 ± 0.01	2.04	n.a.	n.a.	<dl	<dl	5.4	5.8	n.a.	112	N/A
EV818 BP2 PW	2.79 ± 0.04	3.01	n.a.	n.a.	<dl	<dl	4.4	4.7	n.a.	132	N/A
EV818 DN2 PW	2.80 ± 0.06	3.16	n.a.	n.a.	<dl	<dl	1.0	1.1	n.a.	148	N/A
EV818 DP2 PW	11.1 ± 0.04	9.90	n.a.	n.a.	<dl	<dl	1.0	0.9	n.a.	202	N/A
KL739 A3N FI	2.17 ± 0.02	6.91	4.4	29.2	0.32	1.03	23 ± 1	106	n.a.	1415 ± 181	0.74
KL739 A3P FI	1.45 ± 0.02	8.67	2.7	30.6	0.12	0.69	9 ± 7	23	n.a.	1380 ± 55	<dl
KL739 B3N FI	1.72 ± 0.05	8.39	5.2	32.4	0.22	1.07	9 ± 2	36	n.a.	856 ± 51	0.09
KL739 B3P FI	1.22 ± 0.07	5.35	3.1	31.2	<dl	<dl	8 ± 2	33	n.a.	791 ± 257	0.054 ± 0.006
KL739 B6N FI	0.84 ± 0.02	4.01	5.9	32.0	<dl	<dl	16 ± 2	72	n.a.	1162 ± 59	0.03
KL739 B6P FI	1.58 ± 0.09	12.6	1.9	29.4	0.39	1.69	19 ± 1	72	n.a.	1332 ± 209	0.56
KL739 A8N FI	6.30 ± 0.16	45.7	3.8	30.4	<dl	<dl	79	573	n.a.	1000	0.59
KL739 A8P FI	0.61	4.1	3.5	29.8	<dl	<dl	85	572	n.a.	1438	n.a.
KL739 A9N FI	3.80 ± 0.16	12.1	3.9	28.0	<dl	<dl	121	388	n.a.	857	0.13
KL739 A9P FI	1.97 ± 0.16	5.03	5.0	33.6	<dl	<dl	119	303	n.a.	968	0.14
KL739 B10P FI	3.13 ± 0.04	9.61	1.0	49.2	0.64	2.14	24	76	n.a.	1339	n.a.
EV224 2 N FI	4.90 ± 0.16	53.1	5.1	27.2	<dl	<dl	12.27 ± 0.01	128	n.a.	833 ± 39	0.25 ± 0.14
EV818 P FI	3.31 ± 0.06	20.0	2.8	41.3	<dl	<dl	40 ± 4	167	n.a.	412 ± 77	1.40
EV818 BN2 FI	14.30 ± 0.04	51.9	n.a.	n.a.	<dl	<dl	5 ± 3	17	n.a.	181	0.76
EV818 BP2 FI	18.70 ± 0.26	61.7	n.a.	n.a.	<dl	<dl	2.8	9.2	n.a.	146	0.37
EV 3 KS 24.4 PW	7 ± 3	7	n.a.	n.a.	0.2 ± 0.3	0.19	26 ± 9	26.4	n.a.	1021 ± 146	N/A
EV 3 KS TZ1 PW	2.9 ± 1.4	4	n.a.	n.a.	1.2 ± 0.6	1.6	25 ± 16	32	n.a.	871 ± 75	N/A
EV 3 TZ2 Paleo PW	9 ± 4	6	n.a.	n.a.	1.2 ± 0.5	0.7	14.9 ± 0.1	9.3	n.a.	263 ± 110	N/A
EV3 Paleo 40.8 PW	10 ± 5	6	n.a.	n.a.	2.0 ± 0.9	1.2	46 ± 9	29	2.9	1534 ± 261	N/A
EV 3 KS 24.4 FI	1.5 ± 0.3	4.9	n.a.	n.a.	0.3 ± 0.3	0.4	7 ± 3	22	n.a.	438 ± 41	2.1 ± 0.8
EV 3 KS TZ1 FI	2.9 ± 1.6	18	n.a.	n.a.	3 ± 3	16	3 ± 2	14	n.a.	1072 ± 187	3.2 ± 1.2
EV 3 TZ2 Paleo FI	1.7 ± 0.8	13	n.a.	n.a.	1.3 ± 0.8	8	6 ± 2	41	n.a.	2304 ± 677	5.8 ± 1.0
EV3 Paleo 40.8 FI	2.1 ± 0.4	8.0	n.a.	n.a.	0.3 ± 0.3	0.8	30 ± 12	116	n.a.	1203 ± 292	3.9 ± 1.9

[a] PW = pore water. FI = fluid inclusion leachate. KL — Kloof Au Mine–Ventersdorp Supergroup metavolcanic. EV — Evander Au Mine Witwatersrand Supergroup quartzite. P = outer core paring. N = internal core nugget. <dl = below detection limit. n.a. = not analyzed. N/A = not applicable.
[b] Measured concentration of species in leachate.
[c] Calculated concentration of species using Eq. (1) in the text.

porosity (or fluid inclusion fractional volume) of the rock and MW_x is the molecular weight of the N species (mg/mM). Rock density and porosity were determined on seven representative 1 in. diameter subcores by Core Petrophysics Inc. (Houston, TX). Fluid inclusion fractional volume was based on thin section examination.

3.5. NO_3^- isotopic measurements

The $\delta^{15}N$–NO_3^- and $\delta^{18}O$–NO_3^- were analyzed using the denitrifier method (Sigman et al., 2001; Casciotti et al., 2002). In this procedure, NO_3^- was quantitatively converted to N_2O using a strain of denitrifying bacteria (*Pseudomonas aureofaciens*) a naturally occurring mutant that lacks the ability to reduce N_2O. The resulting N_2O was extracted, purified and introduced into isotope ratio mass spectrometer (ThermoFinnigan DeltaPlus). Each analysis was referenced to injections of N_2O from a pure N_2O gas cylinder and then standardized using an internationally accepted NO_3^- reference material (IAEA-N3, with a $\delta^{15}N$ of 4.7‰ AIR and a $\delta^{18}O$ of 25.6‰ VSMOW) with corrections for water–oxygen atom incorporation using the same reference material dissolved in ^{18}O-enriched water (Casciotti et al., 2002). Analytical precision at the time of analyses was typically ±0.5‰ for $\delta^{18}O$ and ±0.2‰ for $\delta^{15}N$ (Tables 1–3 and 5).

3.6. Solid N and C isotopic analyses and total U analyses

Rock core chunks were crushed under a He atmosphere in an anaerobic chamber and 15 to 20 mg were transferred to Sn capsules, which were then sealed. Samples were then introduced into the autosampler (A2100) of a Carlo Erba Instruments, NA 2500 series, elemental analyzer (EA) (Wooller et al., 2001), where N_2 and CO_2 are obtained by combustion at 1020 °C. The elemental composition is reported as total nitrogen, N and total carbon, TC in moles. The $\delta^{15}N$ and $\delta^{13}C$ of the total N and C of the rock, $\delta^{15}N$–N and $\delta^{13}C$–C, were measured using continuous-flow, stable isotope ratio mass spectrometry (Finnigan MAT, Delta^{plus}XL at the Geophysical laboratory, CIW) relative to internal working gas standards (Wooller et al., 2003; Papineau et al., 2009). Precision for $\delta^{15}N$–N was ±0.5‰ AIR for samples with more than 1 μg of N and ±1.2‰ AIR for samples with less than 1 μg of N and for $\delta^{13}C$–C was ±0.1‰ VPDB. Only the $\delta^{15}N$–N of those samples with >0.5 μg of N are considered precise enough for constraining the isotopic composition of the total rock N. Samples were also acidified with ultra-pure 6 N HCl, spun down, rinsed with DI water, dried, weighed and combusted in order to obtain the concentration and the $\delta^{13}C$ of the organic carbon, $\delta^{13}C$–OC. The concentration was determined by subtracting the OC from the TC; and the $\delta^{13}C$ of the inorganic carbon, $\delta^{13}C$–IC, was determined from the isotopic mass balance (Table 4).

An 80 mg portion of pulverized paring and nugget was dried overnight in an oven at 120 °C. $LiBO_3$ powder was added to the sample at a 5:1 ratio ($LiBO_3$:sample). After the powders were mixed carefully they were transferred to a pre-ignited graphite crucible, which was placed in an oven at 1100 °C for 10 min. The molten sample was then quickly poured into a 250 mL Teflon beaker with 40 mL 2:25 HNO_3 and a stir bar, placed on a stirrer and covered with a watch

Table 4
Rock core N and C data.

Sample	Rock type	Bulk density g cm^{-3}	Por. %	U (ppm)	Total N[a] 10^{-3} mol kg^{-1}	$\delta^{15}N$ N (‰)[b]	Organic carbon[c] 10^{-2} mol kg^{-1}	$\delta^{13}C_{org}$ (‰)[c]	Inorganiccarbon[d] 10^{-2} mol kg^{-1}	$\delta^{13}C_{inorg}$ (‰)[b]
EV 3 KS TZ2-Paleo	Kimberley Shale-sltst.	n.a.	n.a.	58 ± 11	3.79 ± 0.47	0.54 ± 0.35	11.9	−28.37	<dl	n.a.
EV 3 KS 1.9	Kimberley Shale-Up. Calc.	n.a.	n.a.	65 ± 6	<dl	n.a.	7.39	−29.97	21.3	−5.62
EV 3 KS 24.4	Kimberley Shale-up. calc. sltst.	2.76	0.5	89 ± 14	2.14 ± 0.16	5.61 ± 4.60	5.06 ± 0.24	−30.17 ± 0.15	1.14 ± 0.54	−6 ± 11
EV 3 KS TZ1	Kimberley Shale-sltst.	n.a.	n.a.	144 ± 3	2.42 ± 0.23	4.93 ± 0.63	2.03 ± 0.21	−25.57 ± 0.25	1.38 ± 0.44	4.1 ± 2.7
EV 3 KS Paleo 40.8	Kimberley Shale-up. laminated	2.78	1.0	108 ± 20	3.57 ± 0.18	6.65 ± 3.83	1.53	−26.4	0.954	−3.83
EV 3 Cong	LK1 reef chert pebble cong.	2.66	0.7	83 ± 6	<dl	n.a.	1.68	−24.16	1.39	−25.92
EV 3 Qtzite	LK1 quartzite	2.64	0.9	19 ± 9	<dl	n.a.	1.06	−25.6	0.521	−19.91
EV 818	Quartzite	2.70	0.6	32 ± 13	1.86 ± 0.49	9.3 ± 12.46	1.81	−25.5	<dl	n.a.
EV 224	Quartzite	2.71	0.6	32	1.14 ± 0.88	−6.2 ± 8.06	2.08	−24.4	<dl	n.a.
KL 739	Metavolcanic w/ calcite veins	2.73	0.7	35 ± 18	1.79 ± 0.93	5.2	2.99 ± 0.96	−25.38 ± 0.27	124 ± 86	−8.3 ± 1.0

[a] Total N ranged from 16 to 53 ppm.
[b] $\delta^{15}N$ values for Total N are expressed in ‰ with respect to atmospheric N_2 and $\delta^{13}C$ for organic carbon and inorganic carbon are expressed in ‰ with respect to V-PDB.
[c] Organic carbon ranged from 127 to 1430 ppm.
[d] Inorganic carbon ranged from 63 to 2520 ppm.

glass for 5 min. The sample was then transferred to a 50 mL volumetric flask and the volume made up to 50 mL with DI water. The U concentration of the solution was measured by ICP-OES (Perkin Elmer) and converted to mol U/kg rock (Table 4).

3.7. Nitrogen isotopic analyses of NH_4^+

NH_4^+ was extracted and analyzed using a protocol described by Houlton et al. (2007) that merges the "passive ammonia diffusion" method for NH_4^+ collection described in Sigman et al. (1997) with the "persulfate/denitrifier" method for analyzing the $\delta^{15}N$ of reduced N forms (Knapp et al., 2005). Briefly, NH_4^+ "traps" were constructed by sealing pre-combusted GF/F filters (with 20 μL of 2 N H_2SO_4 added to each filter) inside Teflon tape envelopes. Between 5 and 40 mL of sample was aliquoted to acid-washed 50 mL Falcon centrifuge tubes. To avoid rupture of the "traps" due to the osmotic pressure gradient between the acidified filters inside the Teflon envelope and the ambient water, a NaCl solution (NaCl was pre-combusted at 650 °C) was added to a final concentration of 0.6 M. The Teflon traps were then added to each tube, followed immediately by addition of 20 to 200 mg, depending on a sample volume, of MgO, pre-combusted at 650 °C, so that the final pH of the fluid sample was ~9.7. The tubes were then immediately capped and incubated at room temperature on a shaker for 8–20 days.

After the incubations, the traps were removed from the tubes, briefly rinsed in deionized water of pH ~3, and stored in tightly capped 4 mL glass vials. Several days later, the filters were removed from the Teflon traps, 3 mL of A.C.S. reagent grade water (Sigma) and 1 mL of POR oxidizing reagent, prepared as described in Knapp et al. (2005), was added to each vial containing a filter. Immediately after addition of the POR reagent, tightly capped vials were autoclaved for 80 min at 120 °C, oxidizing NH_4^+ trapped on a filter to NO_3^-. After autoclaving, [NO_3^-] was determined as described above. Only samples with a final NO_3^- yield greater than 50% of the original NH_4^+ concentration were analyzed for $\delta^{15}N$–NH_4^+ (Table 1). Unfortunately, due to the long storage time between the original core extractions and analyses, only one fluid inclusion extract met this criterion (Table 3). Simultaneous with samples, NH_4^+ extraction was performed on a set of standards prepared from $(NH_4)_2SO_4$ salts (isotopic reference materials IAEA-N1 and IAEA-N2). Based on the standards, the average yield for the ammonium extraction procedure was 95 ± 14% (n = 8). Procedural blank of 16 ± 3 nmol (n = 3) was determined by carrying out the extraction procedure with deionized water with NaCl, MgO and traps added, and constituted 4–15% of a sample or standard. A correction was applied to the measured $\delta^{15}N$–NH_4^+ values using the procedural blank $\delta^{15}N$, derived from the isotopic mass balance between the measured and expected $\delta^{15}N$ of the standards. For example, average measured $\delta^{15}N$ of IAEA-N2 (reported $\delta^{15}N$ = 20.4 ± 0.2‰) was 17.5 ± 0.1‰ (n = 2) and 18.8 ± 0.2‰ (n = 2) for standards containing 200 and 400 nmol of N, respectively, while average measured $\delta^{15}N$ of IAEA-N1 (reported $\delta^{15}N$ = 0.4 ± 0.1‰) was −1.2 ± 0.1‰ (n = 2) and 0 ± 0.1‰ (n = 2). Average $\delta^{15}N$ composition of the procedural blank determined using both standards (IAEA-N1 and IAEA-N2) was applied to obtain final $\delta^{15}N$–NH_4^+ values.

3.8. N_2 compositional and isotopic analyses

Compositional and isotopic analyses of N_2 gas samples dissolved in the fracture water were performed at the Stable Isotope Laboratory at the University of Toronto using the method of Ward et al. (2004). A Varian 3800 GC equipped with a micro-thermal conductivity detector (μTCD) and a Varian Molecular Sieve 5A PLOT fused silica column (25 m × 0.53 mm ID) were used to determine the N_2 concentrations. All analyses were run in triplicate and mean values are reported. Reproducibility for triplicate analyses was ±5%.

The concentrations of dissolved gases were derived from the gas volume abundance, the ratio of water to gas flow rates and Henry's Law constants following the procedure of Andrews and Wilson (1987). The N_2 data was first corrected for air contamination based on the O_2 concentration, which was assumed to be an artifact of sampling, since Eh measurements indicated highly reducing borehole environments. N_2/Ar or O_2/Ar ratios cannot be used as a second crosscheck on contamination due to the radiogenic-rich Ar isotopic signature and the depleted atmospheric Ar concentrations reported by Lippmann et al. (2003). The air correction was made using the following equation,

$$\%N_{2(CORR)} = \%N_{2(MEAS)} - 3.73 \cdot \left(\%O_{2(MEAS)}\right). \tag{2}$$

The dissolved N_2 concentration was calculated according to the following equation,

$$N_2 = \left(V_g/V_w\right) \cdot \%N_{2(CORR)} \cdot 10^{-2} \cdot P/(0.082054 \cdot T) + \%N_{2(CORR)} \cdot 10^{-2} \cdot P \cdot H/18000 \tag{3}$$

where N_2 is in mol L^{-1}, V_g and V_w are the gas and water flow rates, respectively, P is the ambient pressure underground in atm, T is the ambient water temperature in K and H is the Henry's Law constant for N_2 in moles of N_2 (moles of $H_2O)^{-1}$ atm^{-1} (Table 1).

The N isotope analyses were performed using a Varian 3400 Chromatogram coupled with a Finnigan 252 mass spectrometer (GC-IRMS). The N_2 was separated from other gases using a Varian Molecular Sieve 5A PLOT fused silica column (25 m × 0.53 mm I.D.) and a He flow rate of 1.2 mL min^{-1}. The temperature program started at 30 °C for 6 min and then ramped up to 230 °C at 20 °C min^{-1}. All N_2 gas analyses were run in triplicate, and mean values are reported as $\delta^{15}N$–N_2 with respect to atmospheric N_2 using laboratory characterized air working standards cross-calibrated against international IAEA nitrogen standard materials. Measured $\delta^{15}N$–N_2 values are reported in Table 1. To attempt to correct for air contamination (and resultant mixing of the fracture gas N_2 with N_2 associated with air contamination during sampling, as discussed above), corrected $\delta^{15}N$–N_2 values were calculated using the following formula,

$$\delta^{15}N - N_{2(\mathrm{AIR\ CORR})} = \left[\%N_2 \cdot d^{15}N{-}N_2\right] / \%N_{2(\mathrm{AIR\ CORR})}. \tag{4}$$

The range of corrected values (−0.9‰ to 5.8‰) is somewhat larger than the range of measured values (−0.9‰ to 2.9‰), but the differences are not large enough to affect the interpretations.

3.9. Irradiation experiments

Aqueous solutions of NH_4Cl were prepared using spectroscopic grade solid salts and deionized H_2O in varying concentrations in an anaerobic glove bag (containing 90% N_2: 10% H_2). Each solution was mixed in a 160 mL serum vial and then injected into separate 30 mL serum vials. With one exception (Solution #4 in Table 1 of Supplemental Information), they were then bubbled with Ar to expel any H_2 or N_2 in the vial. Anaerobic NaOH solution was added to some of the serum vials in order to bring their pH to 10. This converted the NH_4^+ to NH_3.

Irradiations were carried out at two separate facilities, the Center for Radiological Research at Columbia Medical School and the Notre Dame Radiation Laboratory. The former had a ^{60}Co gamma source with a LET of 0.2 and a dose rate of 0.36 Gy s^{-1}, whereas the latter had a ^{137}Cs source with an LET of 6.5 and dose rate of 0.2 Gy s^{-1}.

Because the concentrations of radiolytically produced NO_3^- were likely to be minute, extreme care was taken to avoid contamination of the solutions. Measurements of NO_2^- and NO_3^- concentration were performed by ion chromatography as described above (Table 2 in Supplemental Section and Table 5). Each set of samples run through the IC was preceded and followed by two blanks of deionized H_2O, and one blank was placed between each sample to ensure there was no cross-contamination and to measure necessary corrections for data (average blank value was subtracted from the total measured concentration). Solutions were frozen shortly after creation and only unfrozen for the purposes of irradiation and analysis and were maintained in a −20 °C freezer between steps. The isotopic composition of the NO_3^- was determined as described above on samples for which the NO_2^- was insignificant (Table 5).

3.10. Irradiation models

Rigg et al. (1952) originally proposed the following equations as the first two steps in the radiolytic oxidation of NH_3.

$$NH_3 + OH \rightarrow NH_2 + H_2O \tag{5}$$

Table 5
$\delta^{15}N$ and $\delta^{18}O$ values of radiolytically produced NO_3^-.

Dose (kGy)[a]	NO_3 (μM)	$\delta^{15}N$ (‰ air)	$\delta^{18}O$ (‰ VSMOW)	$\Delta^{18}O$–NO_3–H_2O (‰)[b]
0	1.89 ± 0.01	1.7	18.1	24.6
30	242.72 ± 0.01	−25.4	9.9	16.4
50	253.85 ± 0.01	−23.8	10.4	16.8
50	222.37 ± 0.01	−22.1	8.9	15.3

[a] ^{137}Cs γ rays at a dose rate of 720 Gy h^{-1} of a pH 7, 50 mM NH_4Cl solution.
[b] Calculated assuming the $\delta^{18}O$ of the milliQ DI water used in the solution was −6.5‰. $\Delta^{15}N$ NO_3–NH_4 is equal to $\delta^{15}N$ of the nitrate, since the $\delta^{15}N$ of the NH_4Cl solution ~0‰.

$$NH_2 + O_2 \rightarrow NH_2O_2 \tag{6}$$

Pagsberg (1972) used pulse radiolysis experiments to prove that NH_2O_2 radicals are formed by the reaction of NH_2 radicals with O_2 and that limited destruction of NH_3 does occur during the irradiation of solutions in the absence of O_2 by forming hydrazine, N_2H_4, by the following reaction.

$$NH_2 + NH_2 \rightarrow N_2H_4 \tag{7}$$

Dwibedy et al. (1996) detected small amounts of NO_3^-, although only in O_2 saturated solutions and only at ~4 kGy. Dwibedy et al. (1996) also observed that NO_2^- yields fluctuated according to concentrations of O_2 and NH_3. T-butanol, an OH scavenger, prevented the accumulation of NO_2^-, signifying that reaction (5) was a necessary first step in the oxidation process. N_2H_4 was not observed as a radiolytic product in air or O_2 saturated NH_3 solutions, leading Dwibedy et al. (1996) to conclude that dimerization of NH_2 does not occur in the presence of O_2 due to the much faster formation of NH_2O_2. Dwibedy et al. (1996) proposed the following reactions as necessary steps in the pathway to NO_2^-.

$$NH_2O_2 \rightarrow NO + H_2O \tag{8}$$

$$4NO + H_2O \rightarrow 2NO_2^- + N_2O + 2H^+ \tag{9}$$

As O_2 is depleted, however, NH_2O_2 becomes the rate-limiting variable so that the rate of reaction (8) eventually decreases. Shin et al. (2001) has proposed that H_2O_2 reacts with NO_2^- to create NO_3^- by the following reaction,

$$H_2O_2 + NO_2^- \rightarrow NO_3^- + H_2O. \tag{10}$$

In this study, the final yields for NO_2^- and NO_3^- from irradiated NH_4Cl solutions of varying pH and dosage levels were used to estimate the rate of reaction (10) by comparing them to those calculated from the integration of the second-order kinetic reactions (5) through (10) over the time span of the irradiation using the Kineticus program (Table 2 of Supplemental Information). In order to apply the yields of NO_2^- and NO_3^- to the in situ oxidation of NH_3 in the subsurface, we utilized the expressions of Lin et al. (2005b) to calculate the dosage rate for the Witwatersrand Supergroup quartzite and Ventersdorp Supergroup metavolcanics from their measured U, Th and K concentration, porosity and density. Mineral–water reactions were modeled with the React module of the Geochemist's Workbench Standard Version 8.0 software package (University of Illinois). Radiolytic reactions were defined as mineral phases, He(s), H_2(s), O_2(s), H_2O_2(s) and H_2O_2(l). The first three phases were dissolved into solution at rates predicted from the dosage rate calculated above. H_2O_2(l) was dissociated into radiolytically generated OH_2^- and H^+ at the rate predicted from the dosage rate. Oxidation of NH_3 to NO_3^- was simulated by the two following first order kinetic redox reactions,

$$2NH_3 + 3.5O_2 \rightarrow NO_3^- + NO_2^- + 2H_2O + 2H^+ \tag{11}$$

$$H_2O_2 + NO_2^- \rightarrow NO_3^- + H_2O \tag{12}$$

where the reaction rates were determined from the Kineticus model.

4. Results and discussion

4.1. Evaluating potential mining contamination

The pore water and fluid inclusion NH_3/NH_4^+ and NO_3^- concentrations of this study (Table 3) overlap those published by Frimmel et al. (1999), which were based upon crush and leach analyses of Ventersdorp Supergroup hydrothermal quartz vein samples (Fig. 1). The difference

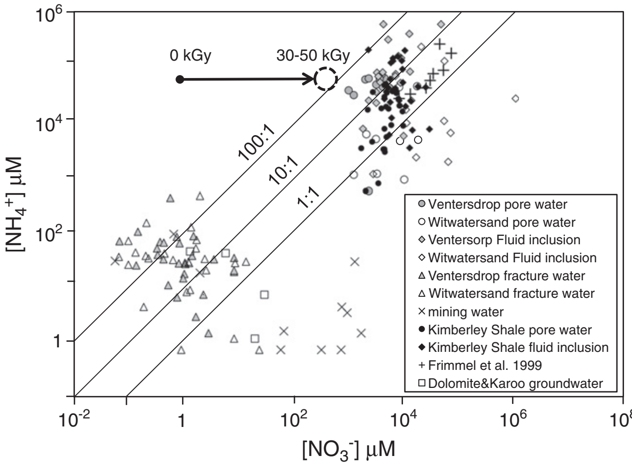

Fig. 1. NH_4^+ versus NO_3^- concentrations for fracture water (triangles), mining water (crosses), ground water from the Transvaal Supergroup dolomite aquifer and the Karoo aquifer (open squares), pore water (circles), and fluid inclusion leachates (diamonds). Gray symbols represent Ventersdorp Supergroup metavolcanic, open symbols represent Witwatersrand Supergroup quartzite and black symbols represent Kimberley Shale. Fluid inclusion data published by Frimmel et al. (1999) are represented by plus signs. Solid arrow illustrates the trend in NH_4^+ and NO_3^- concentrations during the radiolysis experiment.

between this study and that of Frimmel et al. (1999) is that our samples represent the Witwatersrand and Ventersdorp Supergroups host rock lithologies. Additionally, the extraction procedure utilized in this study scrupulously avoided exposing the rock samples to O_2 during the extraction process. This study also utilized core samples that were collected 10 to 50 m beyond the typical tunnel damage zone radius of 2 to 3 m where NO_x-bearing explosive residues in microfractures might be expected to reside (Rubel et al., 2002). Despite these differences, the results from this study are consistent with those of Frimmel et al. (1999) and suggest that NO_3^- does occur within fluid inclusions. The NO_3^- concentrations are ~30 times less than the NH_3/NH_4^+ concentrations in the fluid inclusion and pore water of the Ventersdorp Supergroup metavolcanics, whereas the NO_3^- and NH_3/NH_4^+ concentrations are approximately equal in the fluid inclusion and pore water of the Witwatersrand Supergroup quartzite (Fig. 1).

The NO_3^- concentration in the fracture water (Table 1) was ~10^4 times less than that in the pore water and fluid inclusions, whereas the NH_3/NH_4^+ concentration in the fracture water was ~10^3 times less than that in the pore water and fluid inclusions (Fig. 1). The NH_3/NH_4^+ and NO_3^- concentrations of the fracture water overlap that of the groundwater in the overlying Karoo and Transvaal Dolomite aquifers and some of the mining water, but most of the mining water yields NO_3^- concentrations that are higher than and NH_3/NH_4^+ concentrations that are lower than those of the fracture water (Table 2; Fig. 1). NH_3 from explosive residues in the mining water can be nitrified to NO_3^- by nitrifiers, which based upon the 16S rRNA gene sequences (Onstott et al., 2003) have been reported in the mining water and, thereby, can account for its high NO_3^- concentrations. Fertilizer NH_4NO_3 has a $\delta^{15}N$–N of -5 to $+8$‰ (Kendall and Aravena, 2000), and since the manufacturing processes of explosives are similar to that of fertilizers, it seems likely that their isotopic signatures should be similar (Spalding et al., 1982; DiGnazio et al., 1998). Most of the mining water samples in this study are characterized by high NH_4^+ and NO_3^- concentrations, $\delta^{15}N$–NO_3^- values ranging from 0 to 7‰ and $\delta^{18}O$–NO_3^- values less than 5‰ (Fig. 2), which is consistent with contamination by explosive residues (Stroes-Gascoyne and Gascoyne, 1998).

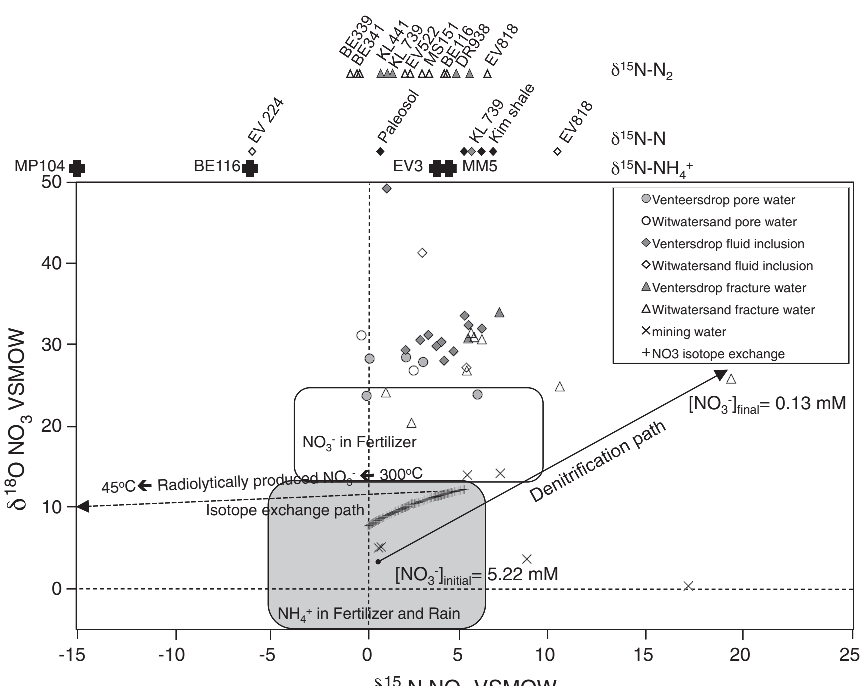

Fig. 2. $\delta^{18}O$–NO_3^- versus $\delta^{15}N$–NO_3^- of fracture water (triangles), mining water (crosses), pore water (circles) and fluid inclusion leachates (diamonds) along with $\delta^{15}N$–N of core samples (diamonds above plot) and $\delta^{15}N$–N_2 of fracture water (triangles above plot) and $\delta^{15}N$–NH_4^+ of fracture water and fluid inclusion water (solid plus signs above plot). Gray symbols represent Ventersdorp Supergroup metavolcanic, open symbols represent Witwatersrand Supergroup quartzite and black symbols represent Kimberley Shale. A hypothetical denitrification line (solid arrow) represents residual NO_3^- as denitrification progresses from an initial 5.22 mM NO_3^- concentration with $\delta^{15}N$–NO_3^- = 0.7‰ and $\delta^{18}O$–NO_3^- = 2.3‰ and $\varepsilon^{15}N = -12$‰ and $\varepsilon^{18}O = -12$‰ (based on Granger et al., 2008) and a final concentration of 0.13 mM. The isotope exchange path of the $\delta^{18}O$–NO_3^- (crosses) is based upon the $\delta^{18}O$–H_2O of the fracture, pore and fluid inclusion water during cooling from $\delta^{18}O$–H_2O = 0‰ at 170 °C at 2.0 Ga to $\delta^{18}O$–$H_2O = -12$‰ at the present day ambient temperature of 45 °C. The path takes into account the kinetic parameters of Bohlke et al. (1997). The distance traversed in $\delta^{15}N$ space is arbitrary and as the path only demonstrates that the $\delta^{18}O$–NO_3^- cannot be explained by isotopic exchange with the $\delta^{18}O$–H_2O. The path of radiolytically produced NO_3^- (dashed line) from 300 to 45 °C is based upon O isotope fractionation measured during radiolysis at room temperature and the $\delta^{18}O$–H_2O of the fracture water. Gray shaded boxes show the range of $\delta^{15}N$–NO_3^- and $\delta^{18}O$–NO_3^- from fertilizer and rain after Kendall and Aravena (2000).

Based upon the concentration data alone, therefore, the NO_3^- present in the fracture water could arise from diffusive exchange with the pore water or mixing with mining water or both. But the distinct difference observed between the $\delta^{18}O$–NO_3^- in the mining water versus the more positive $\delta^{18}O$–NO_3^- in the fracture water, which overlaps that of the fluid inclusion and pore water, clearly indicates that in most cases the fracture water NO_3^- originates from diffusive exchange with the pore water and decrepitation of fluid inclusions and not from contamination due to the explosives used in mining (Fig. 2). Recent results from analysis of noble gases dissolved in the fracture water and fluid inclusions also indicate that much of the fracture water Ne originates from Ne from the 2 Ga fluid inclusions via fluid inclusion leakage and decrepitation (Lippmann-Pipke et al., 2011).

Mining water with high NO_3^- concentration injected into diamond drill holes prior to blasting can penetrate fractures and undergo microbial denitrification in situ as noted by Onstott et al. (2003). Because the O-to-N ratio of isotope fractionation by microbial denitrification is ~1 (Granger et al., 2008), however, elevation of $\delta^{15}N$–NO_3^- and $\delta^{18}O$–NO_3^- of the DR 938 mining water NO_3^- ($\delta^{15}N$–NO_3^- = 0.7‰ and $\delta^{18}O$–NO_3^- = 2.3‰) by denitrification would not yield values that coincide with those of the pore water, the fluid inclusion leachate and most of the fracture water NO_3^- (Fig. 2). Moreover, given ^{15}N and ^{18}O isotope effect amplitudes of up to 30‰ for denitrification (Vogel et al., 1981; Granger et al., 2008), the residual NO_3^- concentrations would also be less than those observed in the pore water (Figs. 1 and 2). No obvious mixing lines between the low salinity mining water and the high salinity pore water and fluid inclusions can explain the fracture water data when the $\delta^{18}O$–NO_3^- is plotted versus the Na^+ concentration (Fig. 3) or, for that matter, when $\delta^{15}N$–NO_3^- is plotted against [NO_3^-], natural log [NO_3^-], or 1/[NO_3^-] (Mariotti et al., 1988). The fracture water, pore water and fluid inclusion NO_3^- isotopic compositions also do not overlap the $\delta^{15}N$–NO_3^- and $\delta^{18}O$–NO_3^- reported for desert NO_3^- deposits (Heaton et al., 1983; Kendall and Aravena, 2000) or for modern precipitation (Hastings et al., 2003). These lines of evidence indicate that trace amounts of NO_3^- present in the fracture water originate from the fluid inclusions and the pore water of the rock formations in the Witwatersrand Basin rather than from the water used in mining.

4.2. Radiolytic generation of NO_2^- and NO_3^-

The pH 10 solutions produced more NO_2^- upon irradiation than pH 7 solutions (Table 2 in Supplemental Section), consistent with NH_3 being the parent for the NO_2^- (reactions (5) through (9)), because the higher pH increases the concentration of NH_3 relative to NH_4^+. The irradiated NO_2^- solution confirms that reaction (10) proposed by Shin et al. (2001) does exist and provides an approximate reaction rate coefficient of ~1 L mol^{-1} s^{-1} for NO_2^- conversion to NO_3^-, which is greater than the rate coefficient for the conversion of NH_3 to NO_2^- (Fig. 4). If the NH_3 concentrations are low, then the NO_2^- is created at a rate slow enough that nearly all produced NO_2^- will be converted to NO_3^-. As pH 7 solutions have ~1% of the NH_3 of pH 10 solutions, the observed NO_2^- concentrations in the pH 7 solutions match the values expected by the radiolytic model. The delayed increase in NO_3^- concentrations (Fig. 5) is consistent with the radiolytic NO_3^- being generated from NO_2^- for which the initial concentrations were negligible. The NO_3^- yields in this study, however, were less affected by the pH than those of the NO_2^-, and this may be because the NO_3^- is also removed from solution by an undetermined radiolytic reaction, but at a rate much slower than that determined for reaction (10) (Table 2 in Supplemental Section; Fig. 4).

The isotopic composition of the NO_3^- found in the irradiated vials was distinct from that of the NO_3^- contamination present in the unirradiated vials, indicating that the NO_3^- was produced by radiolysis (Table 5). The $\delta^{15}N$–NO_3^- of −22 to −25‰ is substantially more negative than that of NH_4Cl ($\delta^{15}N$–NH_4^+ ~0‰), but similar to what would be expected for NH_3 given the −19‰ determined experimentally for the $\Delta^{15}N$ (NH_4^+–NH_3) at room temperature (Hermes et al., 1985). This

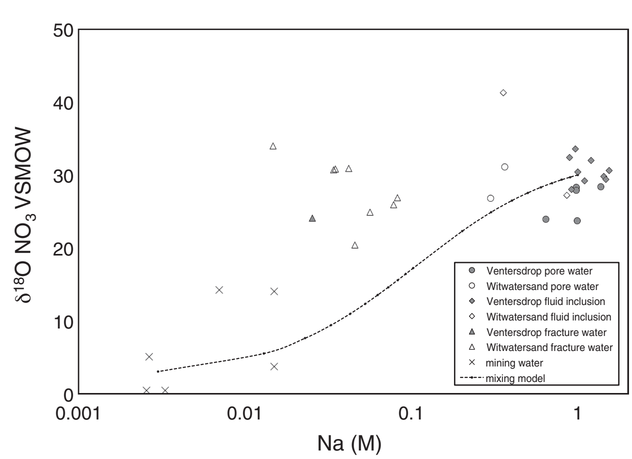

Fig. 3. $\delta^{18}O$–NO_3^- versus [Na^+] for the fracture water, mining water, pore water and fluid inclusions. Symbols are the same as in Fig. 1. The dashed line is mixing line between mining water (3 mM, $\delta^{18}O$–NO_3^- = 3‰) and fluid inclusion NO_3^- (1 M, $\delta^{18}O$–NO_3^- = 30‰).

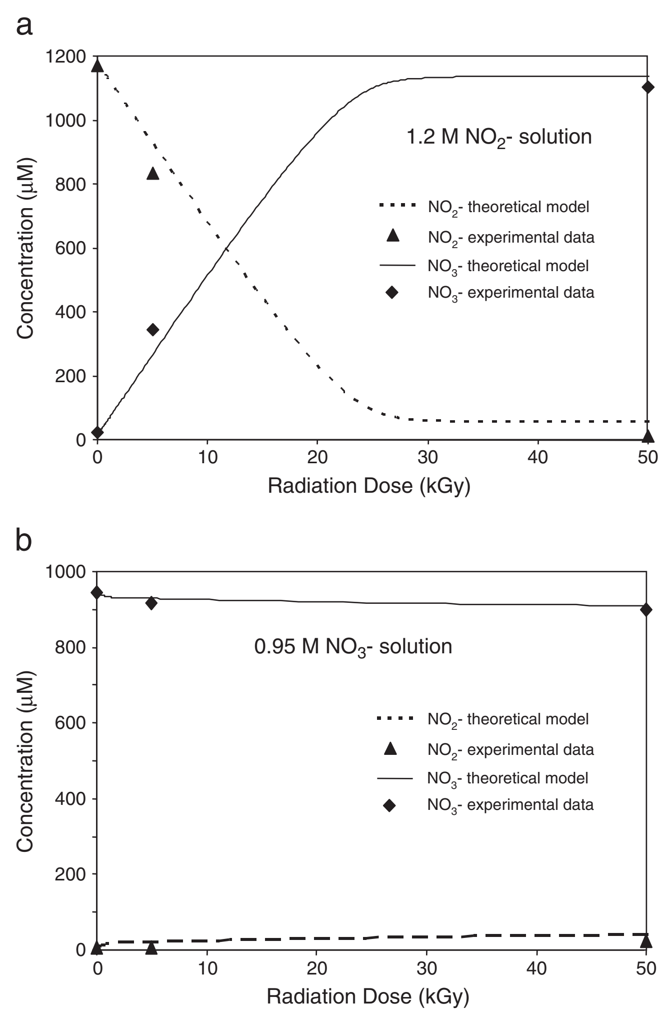

Fig. 4. NO_2^- and NO_3^- concentrations versus dosage a. for a 1.15 mM NO_2^- solution, and b. for a 0.95 mM NO_3^- solution. Model of the NO_2^- (dashed line) and NO_3^- (solid line) concentrations for irradiation of NO_2^- and NO_3^- solutions are superimposed.

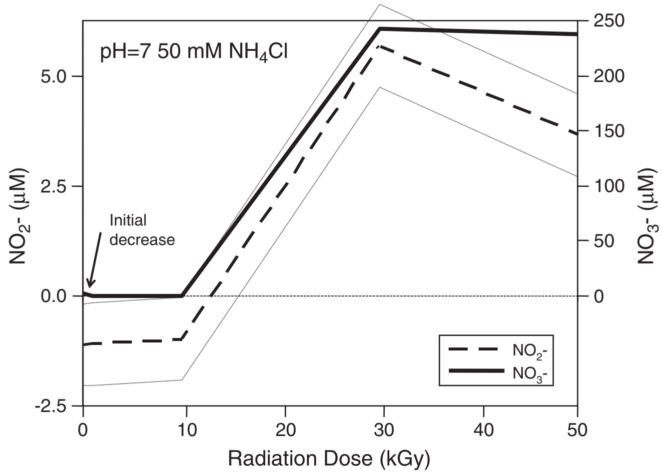

Fig. 5. NO_2^- (dashed line) and NO_3^- (solid line) concentrations versus dosage in kGy for 50 mM NH_4Cl solution of pH 7.2 (solution #8 in Table 1 of Supplemental Data). NO_2^- is plotted with 1 S.D. (dashed line), whereas NO_3^- standard deviation is smaller than the symbol.

verifies that the radiolytically produced NO_3^- was likely to have originated from NH_3 via reaction (5).

The observed $\Delta^{18}O$ values of NO_3^-–H_2O in irradiated solutions were lower than the ~23‰ equilibrium fractionation predicted for 298 K by Bohlke et al. (2003). The $\delta^{18}O$–NO_3^- of contaminating NO_3^- in the unirradiated NH_4Cl solution, however, was consistent with this value and with that of industrial NO_3^- (IAEA-N3 has a $\delta^{18}O$–$NO_3^- = 25.6$‰). The oxygen isotopic analyses suggest that reactions (11) and (12) may have a significant kinetic oxygen fractionation effects associated with them.

If we assume that the net production of radiolytically produced NO_3^- in our experiments can be approximated by Eqs. (11) and (12) alone, then the theoretically estimated O_2 and H_2O_2 concentrations during the radiolysis experiments and the measured NH_3 and NO_2^- concentrations constrain the NO_2^- and NO_3^- production rates to be 0.6 to 2×10^{-10} and 5 to 8×10^{-9} mol L^{-1} Gy^{-1}, respectively, for the pH 7 radiolysis experiments where the NH_3 concentration was ~2.5×10^{-4} mol L^{-1} or ~2.0 to 3.2×10^{-5} mol of NO_3^- L^{-1} (mol of NH_3 $L^{-1})^{-1}$ Gy^{-1}. Using the fluid inclusion salinities (Table 3), porosities, densities, U concentrations (Table 4), and published K and Th concentrations for the Witwatersrand Supergroup quartzite and Ventersdorp Supergroup metavolcanic strata, respectively (Nicolaysen et al., 1981), the relationships of Lin et al. (2005a) yield dosage rates of 5×10^{-12} and 6×10^{-12} Gy s^{-1} for the Witwatersrand Supergroup quartzite and Ventersdorp Supergroup metavolcanic strata, respectively. The NO_3^- production rates corresponding to these dosage rates are 1 to 2×10^{-16} mol of NO_3^- L^{-1}(mol of NH_3 $L^{-1})^{-1}$ s^{-1}. At these production rates, a 1 mM NO_3^- concentration would require ~17 to 32 myr to be produced from a 10 mM NH_3 fluid.

In the presence of Fe^{2+}, NO_2^- and NO_3^- will form NH_3 (Summers and Chang, 1993) at rates of 4.2×10^{-5} and ~5×10^{-5} (mol Fe^{2+} $kg^{-1})^{-1.8}$ s^{-1} at 40 °C in the absence of denitrifying microorganisms, respectively, although their NO_3^- reduction rate is poorly constrained. For the fluid inclusions, these reaction rates are comparable to the radiolytic NO_2^- and NO_3^- production rates. The rapid abiotic production of N_2O also occurs through the reduction of NO_2^- by Fe^{2+} (Samarkin et al., 2010). The available pool of Fe^{2+} in the fluid inclusions, however, is small, and direct oxidation of Fe^{2+} to Fe^{3+} by radiolysis also occurs (Min and Katsumura, 1997). As a result these reactions relatively quickly diminish the Fe^{2+} concentrations to the point that the NO_2^- and NO_3^- reducing reactions become energetically unfavorable and radiolytically produced NO_3^- would steadily accumulate in the fluid inclusions over geological time.

4.3. The origin of the $\delta^{18}O$–NO_3^-

To determine whether the highly positive $\delta^{18}O$–NO_3^- observed in the fluid inclusions, pore water and fracture water could be the result of isotopic exchange with fluid inclusion water over geological time, the temporal evolution of the fluid inclusion $\delta^{18}O$–H_2O was constrained using the $\delta^{18}O$ data for fracture minerals (Zhao et al., 2006), the published fracture water $\delta^{18}O$–H_2O, the basin's thermal history (Omar et al., 2003) and the water/mineral equilibration model of Onstott et al. (2006). This data indicate that the $\delta^{18}O$–H_2O was 5 to 6‰ at 2.0 Ga when the temperature of the fluid was 300 °C (Zhao et al., 2006) and the pH was ~5.5 and the $\delta^{18}O$–H_2O decreased to the present day value of −12‰ (Ward et al., 2004) for saline fracture water at temperatures of 40 °C and pH values of ~7.5 to 8.5 (Onstott et al., 2006). Using the kinetic and isotope exchange parameters of Bohlke et al. (2003), which are sensitive to temperature, pH and salinity, the corresponding temporal variation of the $\delta^{18}O$–NO_3^- was modeled and found to range from 8 to 12‰ (Fig. 2). At temperatures greater than 160 °C the rate of isotopic exchange was fast enough for complete oxygen isotopic equilibration to occur in 10 million years, but the $\Delta^{18}O$ for isotopic equilibrium was only ~6‰ and the maximum $\delta^{18}O$–NO_3^- would be 12‰ (Fig. 2). Over the last 50 million years when the ambient temperatures yielded a larger $\Delta^{18}O$ for isotopic equilibrium, the kinetic rates for isotopic exchange were much slower but the $\delta^{18}O$–H_2O became increasingly more negative resulting in a $\delta^{18}O$–NO_3^- of only 8‰ (Fig. 2). The elevated $\delta^{18}O$–NO_3^- of the fracture, pore and fluid inclusion water, therefore, cannot be reproduced by oxygen isotopic equilibration of the NO_3^- with the fracture water over the last 2.0 byr (Fig. 2).

Assuming a $\delta^{18}O$–H_2O for the hydrothermal solution of 5 to 6‰ (Zhao et al., 2006) and assuming that the measured radiolytic isotope effect, $\Delta^{18}O$–H_2O–$NO_3^- = +16$‰, applies at this temperature, the $\delta^{18}O$–NO_3^- would be ~21to 22‰, close to but still somewhat less than the observed values (Fig. 2). The $\delta^{15}N$–NO_3^- would reflect the NH_3/NH_4^+ and the $\Delta^{15}N$–NH_4^+–NH_3, which ranges 13 to 39‰ from temperatures of 300 to 45 °C. Geochemical modeling indicates that NH_3/NH_4^+ would have been 4 at 300 °C and assuming that its $\delta^{15}N$ equaled that of the Kimberley Shale, 6‰, the $\delta^{15}N$–NO_3^- produced by radiolysis of the NH_3 would have been 3‰ closed to that observed. As the hydrothermal fluid cools over time and the NH_4^+–NH_3 boundary increases to a pH of 8.5, greater than that of the fracture water pH, and NH_4^+ becomes the dominant species, the $\Delta^{15}N$–NH_4^+–NH_3 increases to 39‰ and the radiolytic NO_3^- production rate declines. The $\delta^{15}N$–NO_3^- produced by radiolysis of the NH_3 would have decreased rapidly and would be −33‰ at 45 °C with a $\delta^{18}O$–NO_3^- of 8‰, quite far away from the observed values (dashed arrow in Fig. 2). As a result, radiolytically produced NO_3^- could approach the observed isotopic composition, but only if the oxygen isotopic equilibration rate was for some reason considerably slower than predicted by the kinetic parameters published by Bohlke et al. (2003).

Two other conceivable sources for the NO_3^- could be NO_2 equilibrating with the hydrothermal fluid or NO_3^--bearing paleometeoric water mixing with the hydrothermal fluid. The former would require a $fO_2 \geq 10^{-28}$, which would seem precluded by the Fe-bearing mineral assemblages observed in the fractures (Drennan et al., 1999). The latter would require extremely high NO_3^- concentrations in the surface precipitation during the mid-Proterozoic, which might be possible if, as proposed by Buick (2007), N_2O was a major greenhouse gas constituent at that time. At 2.0 Ga any biosphere associated with the paleosurface of the Witwatersrand Basin would have been eradicated by the meteoritic impact that led to the formation of the Vredefort Complex, hydrothermal fluid circulation and sterilization of the crust and with it any potential NO_3^--reducing microbial communities. The kinetic parameters of Bohlke et al. (2003) would still predict that the $\delta^{18}O$–NO_3^- of both of these sources would have equilibrated with the $\delta^{18}O$–H_2O at that time. One final possibility is that the abiotic reduction of NO_3^- by Fe^{2+} oxidation produces an isotopically fractionated residual NO_3^- highly enriched with ^{18}O since these reactions do take place at temperatures below which isotopic equilibration of the $\delta^{18}O$–NO_3^- with the $\delta^{18}O$–H_2O would not be significant, but in so doing the NO_3^- should be highly enriched with ^{15}N, which does not seem to be the case.

The similarity of the fracture water NO_3^- isotopic composition with that of the pore water indicates that if dissimilatory NO_3^- reducing microorganisms in the fracture water are producing either N_2 or NH_3 from the NO_3^- diffusing out from the pore water, then they are doing so without significant isotopic fractionation (Fig. 2). This would be expected for high degrees of NO_3^- consumption (Mariotti et al., 1981) in an environment in which the flux of NO_3^- is very slow and diffusion limited.

4.4. The NH_3 and N_2 sources

The 25 ± 22 mM NH_3/NH_4^+ average pore water concentration overlaps those reported for oil reservoirs by Manning and Hutcheon (2004). The shale to rock ratio in the Witwatersrand Supergroup is 0.56% (Tweedie, 1986), however, so the origin of the NH_3/NH_4^+, whether it is derived internally from the shale formations or by biological fixation of N_2, bears some consideration. The total N, as measured by combustion, was compared to the summation of N from the various components, ${NH_4^+}_{ex}$, ${NH_4^+}_{FI}$, ${NH_4^+}_{PW}$, ${NO_3^-}_{FI}$, ${NO_3^-}_{PW}$, (Table 6). The calculations reveal that the N mass balance was conserved on all samples within 1 S.D. of reproducibility, with the exception of EV3 TZ2 Paleo, the sample with the highest N and OC concentration (Table 4). The mass balance reveals that more than 90% of the total N in the Kimberley Shale was ${NH_4^+}_{ex}$, presumably residing in the phyllosilicates. In the Witwatersrand Supergroup quartzite samples, the ${NH_4^+}_{ex}$ comprises 32 to 74% of the total N with the ${NH_4^+}_{FI}$ making up 17 to 54% and the ${NO_3^-}_{FI}$ comprising 5 to 10%. In the Ventersdorp Supergroup volcanic samples the ${NH_4^+}_{ex}$ comprises 26% of the total N, with the ${NH_4^+}_{FI}$ making up 57%, the ${NH_4^+}_{PW}$ comprising 13% and the ${NO_3^-}_{FI}$ and ${NO_2^-}_{FI}$ making up only 2% and 1%, respectively. Overall, more than 90% of the N in the studied rock units is NH_4^+ and no more than 10% of the N is found as NO_3^-, and this primarily in the Witwatersrand Supergroup quartzite.

The sample with the highest N and OC content, EV3 TZ2 Paleo, yields a δ^{15}N–N value of 0.5 ± 0.4‰, whereas most of the remaining Kimberley Shale, Witwatersrand Supergroup quartzite and Ventersdorp Supergroup metavolcanic samples yield isotopically heavier δ^{15}N–N values of ~5‰ (Table 4; Fig.2). Comparison of the δ^{13}C–OC with the δ^{15}N–N values of the Kimberley Shale reveals no correlation (Supplementary Figures). Although the ~5‰ δ^{15}N–N values overlap the 1–7‰ δ^{15}N–N values reported by Garvin et al. (2009) for the 2.5 Ga Mount McRae Shale, the Kimberley Shale OC concentrations (127 to 1430 ppm) are than 10 to 100 times less than those reported for the Mount McRae Shale (~18,000 to 161,000 ppm). We therefore cannot preclude the possibility that much of the NH_4^+ originally present in the organic matter of the Kimberley Shale has been volatilized to NH_3 or converted to N_2 during lower green schist facies metamorphism at ~300 °C, thereby increasing the δ^{15}N–N of the residual N. The fact that the NH_4^+ and NO_3^- concentrations of the pore water and fluid inclusions for the Ventersdorp Supergroup metavolcanic and the Witwatersrand Supergroup quartzite do not correlate with their measured OC content is consistent with mobilization of the N during metamorphism.

Assuming a premetamorphic OC content of 1.5 ± 0.5% for the Kimberley Shale (Gray et al., 1998) and a microbial C:N ratio of 7.5 (Vrede et al., 2002), the primary organic N content of the Kimberly Shale would have been $1.7 \pm 0.6 \times 10^{-1}$ mol N kg^{-1} compared to the measured amount of $2.3 \pm 0.2 \times 10^{-3}$ mol N kg^{-1}, which suggests that almost all of the organic N was mobilized. Presumably this N would initially be NH_4^+ in the hydrothermal fluid and partially convert to N_2 (at $fO_2 = 10^{-38}$ to 10^{-28}), to NH_3 (if $fO_2 < 10^{-38}$), or NO_2 (if $fO_2 > 10^{-28}$) (Fig. 6). The presence of pyrite and pyrrhotite in the hydrothermal vein mineral assemblages constrain the fO_2 to be 10^{-31} to 10^{-32} for 300 °C consistent with N_2 formation and Drennan et al. (1999) reported subpopulations of the fluid inclusions containing as much as 10% N_2. The N_2-bearing fluid inclusion could be the source of some of the excess N_2 measured in the fracture water, just as some of the Ne in the fracture water originates from the fluid inclusions (Lippmann-Pipke et al., 2011).

From Table 6 the average total N measured for the Witwatersrand and Ventersdorp Supergroup units is $1.6 \pm 0.4 \times 10^{-3}$ mol N (kg rock)$^{-1}$. When the average fracture water NO_3^- (0.96 +3.2/−0.7 μM), NH_4^+ (20 +78/−16 μM) and N_2 (1000 +3500/−850 μM) concentrations (Table 1) are converted to mol (kg rock)$^{-1}$ assuming an average porosity of 1% and an average density of 2.7 kg L^{-1}, they total 4.3 (+13/−3.2) × 10^{-6} mol N (kg of rock)$^{-1}$, which is insignificant compared to the N contained within the rock matrix. Tweedie (1986) determined a shale/rock (kg kg^{-1}) value of 5.6×10^{-3} for Evander Basin. Multiplying the $1.7 \pm 0.6 \times 10^{-1}$ mol N (kg shale)$^{-1}$ lost during alteration and metamorphism by this factor yields $0.9 \pm 0.3 \times 10^{-3}$ mol N (kg rock)$^{-1}$, a value that is less than the measured values, but not significantly less given the possible errors in the assumptions.

The δ^{15}N–N of the Kimberley Shale samples (4.93 to 6.65‰) and the Ventersdorp Supergroup metavolcanic sample (5.2‰) fall within the range of values reported for lower green schist facies phyllites (3.2 to 7.8‰) in Haendel et al. (1986). In the case of the Witwatersrand strata the total N is comprised primarily of NH_4^+. The most abundant N species in the fracture water was N_2, not NH_4^+, and its δ^{15}N–N_2 values ranged from −1.3 to 5.1‰ (Table 1). The fractionation between our corresponding rock and fluid samples ($\Delta^{15}N = \delta^{15}N$–$N_2$ − δ^{15}N–N) lies between −6.4 (EV818 = 2.9–9.3) to −4.3‰ (KL739 = 0.9–5.2), which overlaps the ranges of −6.0 to −11.5‰ reported by Bottrel et al. (1988) for rock/mineral-fluid inclusion pairs in low-grade metasedimentary rocks. These fractionation values are significantly less than those observed for the experimental results of Li et al. (2009), which ranged from −15 to −19‰ ($\Delta^{15}N = \delta^{15}N$–$N_2$ − δ^{15}N–NH_4^+) and represent kinetic isotopic depletion.

Table 6
Rock N mass balance.

	NO_3^- PW[a] × 10^{-5}	NH_4^+ PW[a] × 10^{-4}	NO_3^- FI[a] × 10^{-5}	NH_4^+ FI[a] × 10^{-4}	${NH_4^+}_{ex}$[a] × 10^{-3}	Σ N[b] × 10^{-3}	N_{meas}[c] × 10^{-3}	N_{meas} − ΣN × 10^{-3}
EV 3 KS 24.4	1.2 ± 0.3	0.48 ± 0.15	1.8 ± 0.2	0.79 ± 0.43	2.1 ± 0.8	2.2 ± 0.9	2.1 ± 0.2	−0.1 ± 1.1
EV 3 KS TZ1	0.65 ± 0.20	0.58 ± 0.31	6.6 ± 4.1	0.67 ± 0.72	3.2 ± 1.3	3.4 ± 1.5	2.4 ± 0.2	−0.9 ± 1.7
EV 3 TZ2 Paleo	2.1 ± 0.9	0.34 ± 0.18	4.6 ± 1.9	1.5 ± 0.6	5.8 ± 1.0	6.0 ± 1.1	3.8 ± 0.5	−2.3 ± 1.6
EV3 Paleo 40.8	2.0 ± 0.9	1.03 ± 0.25	2.6 ± 0.6	4.2 ± 1.6	3.9 ± 1.9	4.4 ± 2.1	3.6 ± 0.2	−0.9 ± 2.3
EV818	0.7 ± 1.0	0.45 ± 0.60	5.2 ± 2.8	1.8 ± 2.7	0.81 ± 0.45	1.1 ± 0.9	1.9 ± 0.5	0.8 ± 1.4
EV224	2.5 ± 1.2	0.098 ± 0.001	7.8 ± 3.9	4.3 ± 2.4	0.25 ± 0.14	0.8 ± 0.5	1.1 ± 0.9	0.4 ± 0.6
KL739	1.4 ± 2.7	1.11 ± 0.57	2.5 ± 3.1	5.0 ± 6.4	0.24 ± 0.22	0.9 ± 1.3	1.8 ± 0.9	0.9 ± 2.2

[a] All units are mol N kg^{-1} rock and are based upon the average values reported in Table 3 multiplied by $\theta_{rock}/\rho_{rock}$.
[b] ΣN is the total mol N kg^{-1} rock from all the listed components.
[c] N_{meas} is from Table 4.

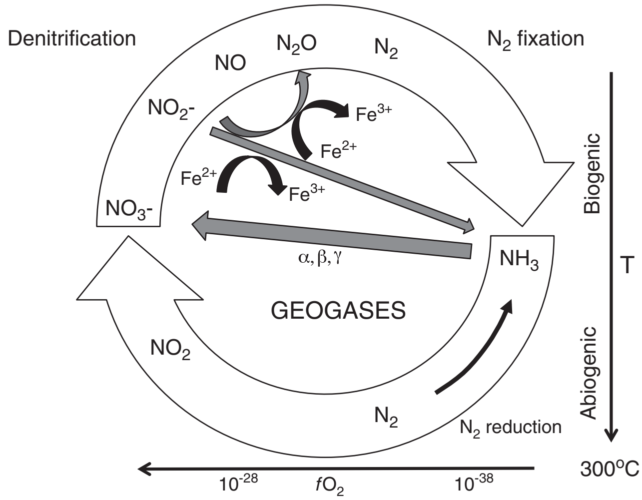

Fig. 6. Conceptual subsurface N cycle split into an upper biogenic and lower abiogenic path (open arrows). NH_3 is oxidized by radiolysis to NO_3^- and NO_2^- (gray arrow), NO_2^- is reduced to NH_3 (smaller gray arrow) via oxidation of Fe^{2+} to Fe^{3+} (small curved black arrow) (Summers and Chang, 1993) and to N_2O (small curved gray arrow) via oxidation of Fe^{2+} to Fe^{3+} (small curved black arrow) (Samarkin et al., 2010). Abiogenic reduction of N_2 and NH_3 is indicated by the black arrow (Brandes et al., 2008). fO_2 values at 300 °C demarcate the boundaries between NO_2, N_2 and NH_3.

If we assume Rayleigh distillation during metamorphism with a kinetic fractionation factor of −5, the average of the observed $\Delta^{15}N$ values, then a +5‰ enrichment in the NH_4^+ in the Kimberley Shale over a presumed initial value of 0‰ would correspond to a loss of 63% of the original total N. The corresponding initial N concentration would then be only 6.3×10^{-3} mol N kg^{-1}, as opposed to the $1.7\pm0.6\times10^{-1}$ mol N kg^{-1} assumed above. The initial N concentration corresponding to the kinetic fraction values of Li et al. (2009) would be even less. The isotopic data indicate that if the nitrogen in Kimberley Shale was transformed to N_2 as suggested by the mineralogical and thermodynamic constraints, then insufficient nitrogen existed within the Kimberley Shale to explain the abundance of nitrogen, primarily NH_4^+, in the Witwatersrand strata and that reduction of N_2 or NO_3^- to NH_4^+ during its geological history is required to explain the observed abundances despite their low values.

The slightly negative values $\delta^{15}N$–N_2 at BE327 H3 and BE325 FW and their low concentrations are consistent with the kinetic fraction model of Li et al. (2009). The $\delta^{15}N$–NH_4^+ values of −6 and −15‰ in the fracture water at Mponeng and Beatrix, however, are difficult to reconcile with simple kinetic fractionation during thermal oxidation of NH_3 to N_2 and would also seem to require a reductive leg to a subsurface N cycle that kinetically fractionates the N isotopes (Fig. 6).

5. Conclusion

The $\delta^{15}N$–NO_3^- and $\delta^{18}O$–NO_3^- isotopic data presented in this study indicate that a subsurface source of NO_3^- exists in the fluid inclusions of the rock strata in Witwatersrand Basin, but the origin of the highly positive $\delta^{18}O$–NO_3^- values requires explanation. In this regard oxygen isotopic analyses of the abiotic reduction of NO_3^- by Fe^{2+} oxidation should be performed to determine the kinetic isotopic fractionation values. Although most of the N retained within the rock matrix as NH_3 either trapped in fluid inclusions or in exchangeable phyllosilicate sites with a minor fraction present as N_2, this NO_3^- source provides a third N nutrient source and an energy-rich electron acceptor to subsurface microbial communities as it leaks out of the inclusions into the pore space and eventually into the fracture water. The $\delta^{15}N$–N, $\delta^{15}N$–N_2 and $\delta^{15}N$–NH_4^+ suggest that the reduction of N_2 to NH_4^+ also must have occurred in the Witwatersrand Basin in order to explain the abundance of NH_4^+, but further analyses of the $\delta^{15}N$–NH_4^+ of the fracture water, pore water and fluid inclusion water are required. Experimental determination of the N isotope kinetic fraction factor for abiotic reduction of N_2 and NO_3^- would provide further constraints on this process. Given that at least one of the genomes of one of the subsurface bacteria does contain N_2-fixing genes, some of this reduction may have also occurred through N_2 fixation. Experimental data indicates that radiolysis can produce NO_3^- from NH_3 under anaerobic conditions at rates that can explain the observed concentrations, but not so easily the observed $\delta^{18}O$–NO_3^- values. If true then radiolytically produced NO_3^- should be found in other continental subsurface sites and could support a complete subsurface N cycle. Further irradiation experiments performed under varying pH conditions are required to fully resolve the complex reactions taking place and to obtain a more reliable estimate of the rate of radiolytic NO_3^- production. If a similar radiolytically sustained N cycle occurs on Mars, then we would expect to find N_2 or N_2O released into the atmosphere from a deep, anoxic subsurface environment whenever N_2 or N_2O clathrates are destabilized, thereby replacing the N_2 lost to space over time (Capone et al., 2006).

Acknowledgments

This work was supported by the NASA Astrobiology Institute through award NNA04CC03A to the IPTAI Team co-directed by LMP and TCO, by National Science Foundation LExEn Program grant EAR-9978267 to TCO and by the NSERC Discovery and Accelerator Programs and Canada Research Chair Funds to BSL. We are indebted to Colin Ralston and Walter Seymore of Evander Au Mine (Harmony Gold Mining Co. Ltd.) and Arnand vanHeerden of Kloof Au Mine (Gold Fields Ltd.) for logistical support in acquiring the cores for this study. We also are grateful to the comments from two reviewers which greatly improved the manuscript.

Appendix A. Supplementary data

Supplementary data to this article can be found online at doi:10.1016/j.chemgeo.2011.11.017.

References

Andrews, J.N., Wilson, G.B., 1987. The composition of dissolved gases in deep groundwaters and groundwater degassing. Geological Association of Canada Special Paper 33, 245–252.
Ballentine, C.J., Sherwood Lollar, B., 2002. Regional groundwater focusing of nitrogen and noble gases into the Hugoton–Panhandle giant gas field, USA. Geochimica et Cosmochimica Acta 66, 2483–2497.
Bau, M., Romer, R.L., Luders, V., Beukes, N.J., 1999. Pb, O and C isotopes in silicified Mooidraai dolomite (Transvaal Supergroup, South Africa): implications for the composition of the Paleoproterozoic seawater and "dating" the increase of oxygen in the Precambrian atmosphere. Earth Planeta Sci Lett 174, 43–57.
Bebout, G.E., Fogel, M.L., 1992. Nitrogen-isotope compositions of metasedimentary rocks in the Catalina Schist, California: implications for metamorphic devolatilization history. Geochimica et Cosmochimica Acta 56, 2839–2849.
Bohlke, J.K., Eriksen, G.E., Revesz, K., 1997. Stable isotope evidence for an atmospheric origin of desert nitrate deposits in Northern Chile and Southern California, USA. Chemical Geology (Isotope Geoscience) 136, 135–152.
Bohlke, J.K., Mroczkowski, S.J., Coplen, T.B., 2003. Oxygen isotopes in nitrate: new reference materials for O-18: O-17: O-16 measurements and observations on nitrate–water equilibration. Rapid Communications in Mass Spectrometry 17, 1835–1846.
Bottrel, S.H., Carr, L.P., Dubessy, J., 1988. A nitrogen-rich metamorphic fluid and coexisting minerals in slates from North Wales. Mineralogical Magazine 52, 451–457.
Braman, R.S., Hendrix, S.A., 1989. Nanogram nitrite and nitrate determination in environmental and biological materials by vanadium (III) reduction with chemoluminescence detection. Analytical Chemistry 61, 2715–2718.
Brandes, J.A., Hazen, R.M., Yoder, J.H.A., 2008. Inorganic nitrogen reduction and stability under simulated hydrothermal conditions. Astrobiology 8, 1113–1126.
Buick, R., 2007. Did the Proterozoic Canfield ocean cause a laughing gas greenhouse? Geobiology 5, 97–100.
Capone, D.G., Popa, R., Flood, B., Nealson, K.H., 2006. Follow the nitrogen. Science 312, 708–709.
Casciotti, K.L., Sigman, D.M., Hastings, M.G., Bohlke, J.K., Hilkert, A., 2002. Measurement of the oxygen isotopic composition of nitrate in seawater and freshwater using the denitrifier method. Analytical Chemistry 74 (19), 4905–4912.

Chivian, D., et al., 2008. Environmental genomics reveals a single-species ecosystem deep within Earth. Science 322, 275–278.
D'Hondt, S., et al., 2004. Distributions of microbial activities in deep subseafloor sediments. Science 306 (5705), 2216–2221.
DiGnazio, F.J., Krothe, N.C., Baedke, S.J., Spalding, R.F., 1998. δ^{15}N of nitrate derived from explosive sources in a karst aquifer beneath the Ammunition Burning Ground, Crane Naval Surface Warfare Center, Indiana, USA. Journal of Hydrology 206, 164–175.
Drennan, G.R., Boiron, M.C., Cthelineau, M., Robb, L.J., 1999. Characteristics of post-depositional fluids in the Witwatersrand Basin. Mineralogy and Petrology 66, 83–109.
Dwibedy, P., Kishore, K., Dey, G.R., Moorthy, P.N., 1996. Nitrite formation in the radiolysis of aerated aqueous solutions of ammonia. Radiation Physics and Chemistry 48 (6), 743–747.
Eaton, A.D., Clesceri, L.S., Greenberg, A.E., 1995. Standard Methods for the Examination of Water and Wastewater. American Public Health Association, American Water Works Association, Water Pollution Control Federation, Philadelphia, PA.
Frimmel, H.E., Hallbauer, D.K., Gartz, V.H., 1999. Gold mobilizing fluids in the Witwatersrand Basin: composition and possible sources. Mineralogy and Petrology 66, 55–81.
Garvin, J., Buick, R., Anbar, A.D., Arnold, G.L., Kaufman, A.J., 2009. Isotopic evidence for an aerobic nitrogen cycle in the latest Archean. Science 323, 1045–1048.
Gascoyne, M., Thomas, D.A., 1997. Impact of blasting on groundwater composition in a fracture in Canada's Underground Research Laboratory. Journal of Geophysical Research-Solid Earth 102 (B1), 573–584.
Granger, J., Sigman, D.M., Lehmann, M.F., Tortell, P.D., 2008. Nitrogen and oxygen isotope fractionation during dissimilatory nitrate reduction by denitrifying bacteria. Limnology and Oceanography 53, 2533–2545.
Gray, G.J., Lawrence, S.R., Kenton, K., Cornford, C., 1998. Nature and origin of carbon in the Archaean Witwatersrand Basin, South Africa. Journal of the Geological Society 155, 39–59.
Haendel, D., Muhle, K., Nitzsche, H.M., Stiehl, G., Wand, U., 1986. Isotopic variations of the fixed nitrogen in metamorphic rocks. Geochimica et Cosmochimica Acta 50, 749–758.
Hallbauer, D.K., 1986. The mineralogy and geochemistry of Witwatersrand pyrite, gold, uranium, and carbonaceous matter. In: Maske, C.R.A.a.S. (Ed.), Mineral Deposits of Southern Africa, pp. 731–752.
Hallbauer, D.K., Kable, E.J.D., 1979. Abstr. 18th Congress Geol. Soc. South Africa. Geological Society of South Africa, Port Elizabeth, South Africa, pp. 176–186.
Hallbauer, D.K., Von Gehlen, K., 1983. The Witwatersrand pyrites and metamorphism. Mineralogical Magazine 47, 473–479.
Hastings, M.G., Sigman, D.M., Lipschultz, F., 2003. Isotopic evidence for source changes of nitrate in rain at Bermuda. Journal of Geophysical Research 108.
Heaton, T.H.E., Talma, A.S., Vogel, J.C., 1983. Origin and history of nitrate in confined groundwater in the western Kalahari. Journal of Hydrology 62, 243–262.
Hermes, J.D., Weiss, P.M., Cleland, W.W., 1985. Use of N-15 and deuterium-isotope effects to determine the chemical mechanism of phenylalanine ammonia-lyase. Biochemistry 24, 2959–2967.
Houlton, B.Z., Sigman, D.M., Schuur, E.A.G., Hedin, L.O., 2007. A climate-driven switch in plant nitrogen acquisition within tropical forest communities. Proceedings of the National Academy of Sciences of the United States of America 4, 8902–8906.
Kelley, D.S., et al., 2001. An off-axis hydrothermal vent field near the Mid-atlantic Ridge at 30°N. Nature 412, 145–149.
Kendall, C., Aravena, R., 2000. Nitrate isotopes in groundwater systems. In: Cook, P., Herczeg, A.L. (Eds.), Environmental Tracers in Subsurface Hydrology. Kluwer Academic Publishers, pp. 261–297.
Knapp, A.N., Sigmann, D.M., Lipschultz, F., 2005. N isotopic composition of dissolved organic nitrogen and nitrate at the Bermuda Atlantic time-series study site. Global Biogeochemical Cycles 19.
Li, L., Cartigny, P., Ader, M., 2009. Kinetic nitrogen isotope fractionation associated with thermal decomposition of NH_3: experimental results and potential applications to trace the origin of N_2 in natural gas and hydrothermal systems. Geochimica et Cosmochimica Acta 73.
Lin, L.-H., et al., 2005a. Radiolytic H_2 in the continental crust: nuclear power for deep subsurface microbial communities. Geochemistry, Geophysics, Geosystems 6. doi:10.1029/2004GC000907.
Lin, L.-H., Slater, G., Sherwood Lollar, B., Lacrampe-Couloume, G., Onstott, T.C., 2005b. The yield and isotopic composition of radiolytic H_2, a potential energy source for the deep subsurface biosphere. Geochimica et Cosmochimica Acta 69, 893–903.
Lin, L.H., et al., 2006. Long-term sustainability of a high-energy, low-diversity crustal biome. Science 314, 479–482.
Lipp, J.S., Morono, Y., Inagaki, F., Hinrichs, K.-U., 2008. Significant contribution of Archaea to extant biomass in marine subsurface sediments. Nature 454, 991–994.
Lippmann, J., et al., 2003. Dating ultra-deep mine waters with noble gases and ^{36}Cl, Witwatersrand Basin, South Africa. Geochimica et Cosmochimica Acta 67, 4597–4619.
Lippmann-Pipke, J., Lollar, B.S., Niedermann, S., Stroncik, N.A., Naumann, R., van Heerden, E., Onstott, T.C., 2011. Neon identifies two billion year old fluid component in Kaapvaal Craton. Chemical Geology 283, 287–296.
Manning, D.A.C., Hutcheon, I.E., 2004. Distribution and mineralogical controls on ammonium in deep groundwaters. Applied Geochemistry 19, 1495–1503.
Mariotti, A., et al., 1981. Experimental determination of nitrogen kinetic isotope fractionation: some principles; illustration for the denitrification and nitrification processes. Plant and Soil 62, 413–430.
Mariotti, A., Landreau, A., Simon, B., 1988. ^{15}N isotope biogeochemistry and natural denitrification process in groundwater: application to the chalk aquifer of northern France. Geochimica et Cosmochimica Acta 52, 1869–1878.
Min, M.-Z., Katsumura, Y., 1997. A possible mechanism of wall-rock hematization in uranium deposits: radiation-induced oxidation of ferrous iron. Geochemical Journal 31.
Mysen, B.O., Fogel, M.L., 2010. Nitrogen and hydrogen isotope compositions and solubility in silicate melts in equilibrium with reduced (N + H)-bearing fluids at high pressure and temperature: effects of melt structure. American Mineralogist 95, 987–999.
Nicolaysen, L.O., Hart, R.J., Gale, N.H., 1981. The Vredefort radioelement profile extended to supracrustal strata at Carletonville, with implications for continental heat flow. Journal of Geophysical Research 86, 10653–10661.
Omar, G., Onstott, T.C., Hoek, J., 2003. The origin of deep subsurface microbial communities in the Witwatersrand Basin, South Africa as deduced from apatite fission track analyses. Geofluids 3, 69–80.
Onstott, T.C., et al., 2003. Indigenous versus contaminant microbes in ultradeep mines. Environmental Microbiology 5, 1168–1191.
Onstott, T.C., et al., 2006. The origin and age of biogeochemical trends in deep fracture water of the Witwatersrand Basin, South Africa. Geomicrobiology Journal 23, 369–414.
Pagsberg, P.B., 1972. Investigation of the NH_2 Radical Produced by Pulse Radiolysis of Ammonia in Aqueous Solution. Danish Atomic Energy Commission, Riso, Denmark.
Pagsberg, P., 2001. Laboratory studies of the reaction between nitrogen dioxide and ammonia in the temperature range of 288–357 K. Bulletin of the Polish Academy of Sciences Chemistry 49, 299–304.
Papineau, D., et al., 2009. High primary productivity and nitrogen cycling after the Paleoproterozoic phosphogenic event in the Aravalli Supergroup, India. Precambrian Research 171, 35–56.
Phillips, G.N., 1988. Widespread fluid infiltration during metamorphism of the Witswatersrand goldfields: generation of chloritoid and pyrophyllite. Journal of Metamorphic Geology 6, 311–332.
Rigg, T., Scholes, G., Weiss, J., 1952. Chemical actions of ionising radiations in solutions. The action of X-rays on ammonia in aqueous solution. Journal of the Chemical Society 10, 3034–3038.
Rubel, A.P., Sonntag, C., Lippmann, J., Pearson, F.J., Gautschi, A., 2002. Solute transport in formations of very low permeability: profiles of stable isotope and dissolved noble gas contents of pore water in the Opalinus Clay, Mont Terri, Switzerland. Geochimica et Cosmochimica Acta 66, 1311–1321.
Samarkin, V.A., et al., 2010. Abiotic nitrous oxide emission from the hypersaline Don Juan Pond in Antarctica. Nature Geoscience 3, 341–344.
Shin, H.S., Kim, Y.R., Ponomarev, A.V., 2001. Influence of sulfite on radiolytic conversion of nitrate and nitrite in dilute aqueous solutions. Mendeleev Communications 1, 21–23.
Sigman, D.M., et al., 1997. Natural abundance-level measurement of the nitrogen isotopic composition of oceanic nitrate: an adaptation of the ammonia diffusion method. Marine Chemistry 57, 227–242.
Sigman, D.M., et al., 2001. A bacterial method for the nitrogen isotopic analysis of nitrate in seawater and freshwater. Analytical Chemistry 73 (17), 4145–4153.
Spalding, R.F., Exner, M.E., Lindau, C.W., Eaton, D.W., 1982. Investigations of sources of groundwater nitrate contamination in the Burbank–Wallula area of Washington, USA. Journal of Hydrology 58, 307–324.
Stevens, T., 1997. Lithoautotrophy in the subsurface. FEMS Microbiology Reviews 20, 327–337.
Stevens, T.O., McKinley, J.P., 1995. Lithoautotrophic microbial ecosystems in deep basalt aquifers. Science 270, 450–454.
Stotler, R.L., et al., 2009. Hydrogeochemistry of groundwaters in and below the base of thick permafrost at Lupin, Nunavut, Canada. Journal of Hydrology 373, 80–95.
Stroes-Gascoyne, S., Gascoyne, M., 1998. The introduction of microbial nutrients into a nuclear waste disposal vault during excavation and operation. Environmental Science and Technology 32, 317–326.
Summers, D.P., Chang, S., 1993. Prebiotic ammonia from reduction of nitrite by iron(II) on the early Earth. Nature 365, 630–632.
Tweedie, E.B. (Ed.), 1986. The Evander Goldfield. Mineral Deposits of Southern Africa, 1. Geol. Soc. S. Afr., Johannesburg, S.A.. 705–730 pp.
van der Westhuizen, W.A., de Bruiyn, H., Meintjies, P.G., 1991. The Ventersdorp Supergroup: an overview. Journal of African Earth Sciences 33, 83–105.
Vogel, J.C., Talma, A.S., Heaton, T.H.E., 1981. Gaseous nitrogen as evidence for denitrification in groundwater. Journal of Hydrology 50, 191–200.
Voicu, G., Hallbauer, D.K., 2005. Determination of the physico-chemical characteristics of hydrothermal fluids from the post-metamorphic Omai gold deposit, Guiana Shield, using analysis of ionic species by crush-leach technique and capillary electrophoresis. Mineralogy and Petrology 83, 243–270.
Vrede, K., Heldal, M., Norland, S., Bratbak, G., 2002. Elemental composition (C, N, P) and cell volume of exponentially growing and nutrient-limited bacterioplankton. Applied and Environmental Microbiology 68, 2965–2971.
Wallmach, T., Meyer, F., 1990. A petrogenetic grid for metamorphosed aluminous Witswatersrand shales. South African Journal of Geology 93, 93–102.
Ward, J.A., et al., 2004. Microbial hydrocarbon gases in the Witwatersrand Basin, South Africa: implications for the deep biosphere. Geochimica et Cosmochimica Acta 68, 3239–3250.
Wooller, M.J., Collins, B., Fogel, M., 2001. The elemental analyzer sample carousel: loading an autosampler made easy. Rapid Communications in Mass Spectrometry 15, 1957–1959.
Wooller, M., Smallwood, B., Scharler, U., Jacobsen, M., Fogel, M., 2003. A study of δ^{13}C and δ^{15}N values in Rhizophora mangle leaves for a multi-proxy approach to mangrove paleoecology. Organic Geochemistry 34, 1259–1275.
Zhang, G., Dong, H., Xu, Z., Zhao, D., Zhang, C., 2005. Microbial diversity in ultra-high-pressure rocks and fluids from the Chinese Continental Scientific Drilling Project in China. Applied and Environmental Microbiology 71, 3213–3227.
Zhao, B., Robb, L.J., Harris, C., Jordaan, L.J., 2006. Origin of hydrothermal fluids and gold mineralization associated with theVentersdorp Contact Reef, Witwatersrand Basin, South Africa: constraints from S, O, and H isotopes. Geological Society of America Special Papers 405, 333–352.